JACS
JOURNAL OF THE AMERICAN CHEMICAL SOCIETY

Article

pubs.acs.org/JACS

Kinetics of Multielectron Transfers and Redox-Induced Structural Changes in *N*-Aryl-Expanded Pyridiniums: Establishing Their Unusual, Versatile Electrophoric Activity

Štěpánka Lachmanová,[†] Grégory Dupeyre,[‡] Ján Tarábek,[§] Philippe Ochsenbein,[∥] Christian Perruchot,[‡] Ilaria Ciofini,*[,⊥] Magdaléna Hromadová,*[,†] Lubomír Pospíšil,*[,†,§] and Philippe P. Lainé*[,‡]

[†]J. Heyrovský Institute of Physical Chemistry of ASCR, v. v. i., Dolejškova 3, 182 23 Prague, Czech Republic

[‡]Université Paris Diderot, Sorbonne Paris Cité, ITODYS, UMR CNRS 7086, 15 rue J-A de Baïf, 75013 Paris, France

[§]Institute of Organic Chemistry and Biochemistry of ASCR, v. v. i., Flemingovo nám. 2, 166 10 Prague, Czech Republic

[∥]Laboratoire de Cristallographie et Modélisation Moléculaire du Solide, Sanofi LGCR, 371 rue du Professeur Blayac, Montpellier 34184 Cedex 04, France

[⊥]PSL Research University, Chimie ParisTech—UMR CNRS 8247, Institut de Recherche de Chimie Paris, 11 rue Pierre et Marie Curie, 75005 Paris, France

Supporting Information

ABSTRACT: A combined electrochemical and theoretical study of a series of pyridinium-based electrophores, consisting of reference *N*-alkyl-2,4,6-triarylpyridiniums (**1**−**3**) and *N*-aryl-expanded pyridiniums (EPs), i.e. *N*-aryl-2,4,6-triarylpyridiniums (**4**−**10**), is presented with the aim of elucidating multifaceted mechanisms underpinning the complex electrophoric activity of fluxional EP systems. Series **1**−**10** constitutes a library of model electrophores showing an incremental variation of their composition, charge, and steric hindrance. By kinetic mapping of the first two heterogeneous electron transfers (ETs) of **1**−**10** and computational mapping, at the density functional theory level, of their electronic and geometrical features in various redox states, it is established that, depending on whether EPs are made of one (**4**, **5**) or two "head-to-tail"-connected pyridinium rings (**6**−**10**), the nature of the redox-triggered distortions (when allowed) is different, namely, *N*-pyramidalization due to hybridization change in the former case versus saddle-shaped distortion originating from conflicting intramolecular interactions in the latter case (**8**−**10**). When skeletal relaxations are sterically hampered, zwitterionic states and electron delocalization with quinoidal features are promoted as alternative relaxation modes. It follows that "potential compression" is changed to "potential expansion" (i.e., a further separation of redox potentials) in single-pyridinium EPs (**4**, **5**), whereas "potential inversion" (i.e., single-step two-electron transfer; **8**−**10**) is changed to stepwise ETs of the Weitz type for two-pyridinium EPs (**6**, **7**). Overall, kinetic rate constants not only consistently indicate the most prominent mechanistic aspects of the reduction pathways of EPs, but they are also instrumental in establishing EPs as a unique class of electrophores.

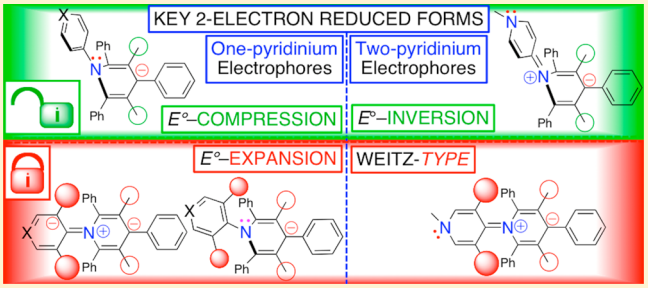

1. INTRODUCTION

Molecular-level transfer of several electrons, whether or not at the same time, i.e. at the same (apparent) potential, is an important phenomenon that operates in many efficient natural processes, in particular in catalytic systems. Understanding its multifaceted mechanism is a challenging task. Multielectron transfers are involved in applications spanning from biosensors and catalysis to solar energy conversion and storage (including man-made photosynthesis) and molecular electronics.[1−4] Organic compounds containing the biorelevant pyridinium motif are suitable models for examination of such electrochemical structure−reactivity relationships. Indeed, in the typical case of the two-electron reduction of a pyridinium core, the process can occur stepwisely or in an apparent single step, depending on the substitution pattern of the electron-accepting cation.[5] Thus, pyridinium derivatives, as (multi)-electron carriers, can function as tunable electrophores.[6]

In the case of the unsubstituted *N*-methylpyridinium cation, the atomic contributions to the LUMO (Chart 1), which governs the first reduction process, originate mainly from the nitrogen atom and carbon atoms in the 2-, 6-, and 4-positions (α- and γ-positions with respect to the nitrogen atom). It is widely accepted that the one-electron-reduced intermediate, the pyridinyl radical, is a reactive species. As a consequence, this pyridinium species acts as an efficient single-electron mediator

Received: May 29, 2015
Published: August 17, 2015

DOI: 10.1021/jacs.5b05545
J. Am. Chem. Soc. 2015, 137, 11349−11364

Chart 1. Pictorial Representation of Weighted Atomic Contributions (open white and solid gray circles) to the LUMO of Pyridinium Rings in Various Chemical Contexts (R = H or alkyl; Ar = aryl)[a]

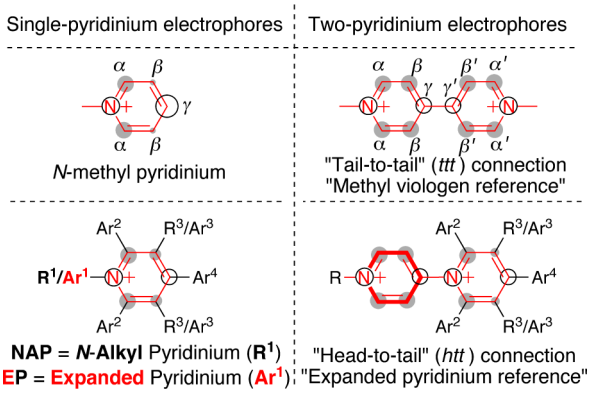

[a]See also the computed LUMO and SOMO orbitals (Figures S1 and S2 in the Supporting Information, along with Figure S3, which shows corresponding spin density maps for one-electron-reduced species).

to substrates. Alternatively, its reactivity leads to the formation of covalent (σ) dimers.[7−12] We recall that the reduction of *N*-methylpyridinium yields the prototypical methyl viologen (MV).[13] An efficient way to eliminate the dimerization is to introduce bulky substituents at the pyridinium positions which contribute the most significantly to the LUMO and to the singly occupied molecular orbital (SOMO), that is to say, the α- and γ-positions (see Chart 1).[14−16] Pyridinium derivatives obtained in this way thus become effective multielectron carriers. When the *N*-pyridinio group differs from a mere alkyl (e.g., methyl) substituent, as is typically the case for 1,2,4,6-polyarylpyridiniums, these electrophores are referred to as (branched) *N*-aryl-expanded pyridiniums (EPs; Chart 1).[6,17,18] At this point, it is worth noting that, despite the lack of steric protection, in dimethyl sulfoxide, MV is reduced in two separate and reversible one-electron steps at −0.37 and −0.70 V against AglAgCl|1 M LiCl reference electrode. In other words, this "tail-to-tail" (ttt) pyridinium dimer is not further involved in a reductive chemical process of (σ) dimerization that could lead to pyridinium oligomers. Further salient features of MV are its remarkable electrochromic properties and the relative stability of its radical cation, which are both well-recognized.[19] These behaviors are ascribed to the delocalized character of the SOMO of the radical cation that shows a typical quinoidal pattern, like the LUMO of MV in its native form (Chart 1). Altogether, these features make MV a popular representative of redox systems of the Weitz type.[19]

In most cases, sterically protected pyridinium derivatives will accept the first two electrons in separate and well-discernible redox steps. Under certain conditions the transfer of these two electrons at the same potential is also possible, as in the typical case of the above-mentioned EPs.[5,6] For such species, conveniently balanced intramolecular steric congestion and the involvement of the orbitals centered on the two pyridinium rings in the LUMO and SOMO, in the case of dicationic "head-to-tail" (htt) bipyridinium derivatives (*htt*-EPs, Chart 1), are instrumental in assisting and/or amplifying structural changes triggered by the first electron transfer (ET) that, in their turn, have a significant impact on the energetics of the second ET process.[5] Indeed, our previous report[5] pointed out the critical role of the redox-induced distortion involving the centrally positioned nitrogen atom. The hybridization change of the N atom of the more congested pyridinium ring, referred to as "the *N*-pyramidalization occurring at the pyridinium core" (see Scheme 1), explains the phenomenon of "potential compression"[20] often observed for single-pyridinium (monocationic) *regular* EPs, that is, branched EPs that are *not* overcongested about the core *N*-pyridinio site. This type of mechanism (Scheme 1) is also invoked[5] to account for the related phenomenon of "potential inversion"[20] that manifests itself experimentally as the above-mentioned transfer of two electrons at apparently the same potential. In the present work, the definitive experimental demonstration is provided that this kind of redox-triggered distortion (although different from *N*-pyramidalization due to a hybridization change in the case of dicationic EPs) is indeed responsible for a characterized inversion of standard potentials.

Scheme 1. Pictorial Representation of Redox-Triggered *N*-Pyramidalization within a Regular Single-Pyridinium (i.e., monocationic) Electrophore of the "Branched" EP Type (e.g., with X = CH) and the Case of a Potential Compression That Involves Two Redox Isomers (electromers) for the One-Electron-Reduced Form[5,a]

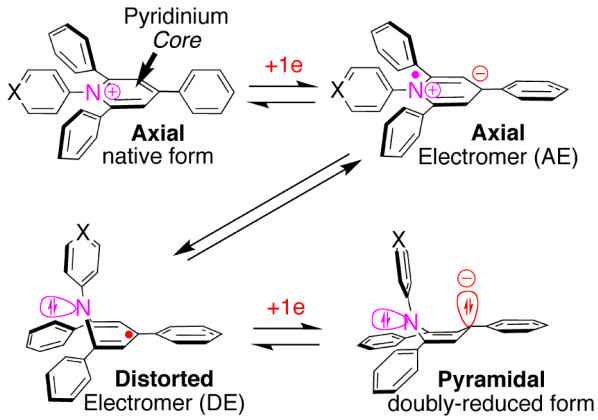

[a]One (AE) retains the axial geometry of the native form, while the other (DE) adopts a *distorted* geometry (here referred to as "pyramidal") close to that of the final two-electron-reduced form.

The observed significant impact of both the steric and the electronic factors on the *energetics* of ET processes led us to anticipate that these factors have also a profound influence on the ET *kinetics* of such electrophores. Gaining detailed knowledge about multielectron processes from in-depth electrochemical study of selected model pyridinium compounds is therefore an important research topic, owing to the ubiquity of multielectron transfers. Besides, there is also a widespread use of pyridinium motifs, either as stand-alone platforms (e.g., electrochemical mediators/relays[21] or catalysts[22]) or as building blocks of extended assemblies. For instance, EP-based electron-acceptor units are exploited not only in the design of versatile betaine dyes[23] and nonlinear optical (NLO) chromophores[24] but also in polyad systems for photoinduced charge separation[25,26] or in redox molecular wires.[27,28] Their implementation is essentially determined by the manner in which they handle charge transfer (CT)[29] and (multi)electron uptake/release. This supposes that their reduction mechanisms are sufficiently well established, and one has to be aware of the complexity of redox processes in pyridinium-based electrophores.[5,30] For instance, beyond noninnocent redox-triggered

DOI: 10.1021/jacs.5b05545
J. Am. Chem. Soc. 2015, 137, 11349−11364

configurational changes, which impact on certain functional principles (e.g., long-range charge delocalization in oligopyridinium wires), the time scale within which the changes occur is an important parameter when the system needs to handle several ETs "at once". Therefore, mapping the kinetic landscape of pyridinium-based versatile electrophores is also of prime interest.

The present work deals with the determination and analysis of standard potentials and ET rate constants of differently congested (mono)pyridinium and *htt*-bipyridinium derivatives in order to assess to what extent intramolecular steric hindrance is a valuable parameter to tune the features of ET processes, including their overall layout (successive or simultaneous ETs) and their intrinsic kinetic rates. The scope of the paper is limited to the simplest case study of the first two ETs, starting from the respective monocationic and dicationic native forms of various model electrophores. These latter were designed in such a way that the interplay of (i) steric hindrance (up to overcongestion), (ii) charge/electronic delocalization (or redistribution), and (iii) structural changes (i.e., relaxation of skeletal geometry) could be addressed, assessed, and tested. Beyond the disentanglement of standard potentials in the complicated case of potential coalescence, the experimental difficulty stems partly from the high rates of ET processes that are encountered in such electrochemical systems along with the sensitivity of kinetic measurements toward adsorption, which required a specific experimental methodology. By combining experimental and computational approaches, we provide insights into the different mechanisms by which the type and level of steric hindrance regulate this electrophoric activity, and we also explain why the net number of attached electrons per electrophore is not a simple function of the number of its constitutive pyridinium subunits. Finally, we introduce the notion of "potential expansion", viewed as the opposite of "potential compression", that is to say, a further separation of standard potentials as compared to the reference situation of a nonconstrained electrophore. As regards the detailed energetics underpinning the limiting case of single-step two-electron transfers within dicationic branched EPs, we unambiguously demonstrate that we are dealing with a genuine potential inversion phenomenon.

2. EXPERIMENTAL SECTION

2.1. Syntheses, Characterization, and General Experimental Details. Materials and syntheses of five new electrophores (compounds **2**−**5** and **7** in Chart 2), along with their full characterization, are provided in the Supporting Information (see sections 10−14). The preparation of the other model electrophores was described previously.[5,6]

2.2. X-ray Crystal Structure Determination. Plate crystals of **5**, i.e. $[Py(Ph)_2\text{-}TP](BF_4)$, were grown from a dichloromethane/hexane mixture. Intensity data were collected at low temperature (113 K) on a Bruker APEX-II diffractometer (IμS, Cu Kα, λ = 1.54178 Å, graphite monochromator) in ω and ϕ scan mode, with a sample-to-detector distances of 40 mm. The data were corrected for Lorentz, polarization, and absorption effects. Crystal data are given in the Supporting Information (see section 3 and the CIF file).

2.3. Electrochemical Measurements. Samples for electrochemical measurements were prepared in dimethyl sulfoxide (DMSO) or in acetonitrile (ACN) using 0.1 M tetrabutylammonium hexafluorophosphate ($TBAPF_6$) as the supporting electrolyte. Two solvents were used in order to distinguish between adsorption-coupled and pure ET kinetics. Even if the ohmic resistance in DMSO was considerably less favorable for measurements at high frequencies, a further reason for using DMSO was the more effective solvation of the molecules studied as compared to that with ACN. Thus, this study required finding a reasonable compromise for the appropriate experimental conditions. The redox potential of the ferrocene/ferrocenium couple against our reference electrode was +0.560 V in DMSO. Instrumentation details are the same as in our previous report[5] and are specified in the Supporting Information (see section 4).

Chart 2. Structural Formulae of the Model Electrophores Here Studied: (top) *N*-Methyl-2,4,6-triarylpyridiniums (1−3) as Well as Branched Expanded Pyridiniums (4, 5) and Bipyridiniums (6, 7) with a Hindered Ar^1 Group That Are Reduced in Two One-Electron Steps and (bottom) Branched, Expanded *htt*-Bipyridiniums That Undergo a Single-Step, Two-Electron Reduction[a]

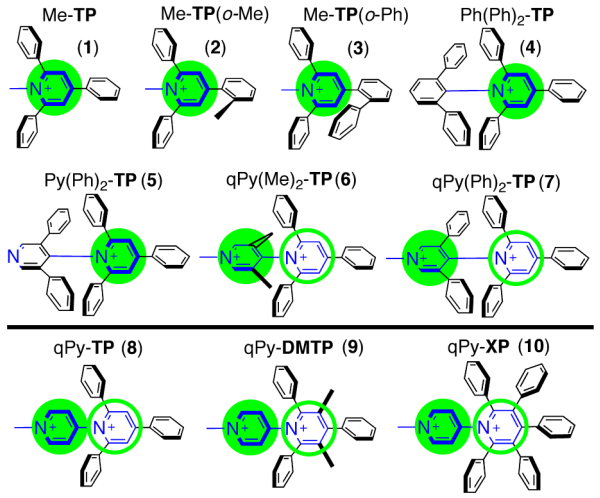

[a]Green zones indicate the relative contribution of the pyridinium rings to the LUMOs (solid = major, open = minor; see Figure S1 in the Supporting Information).

2.4. Electron Paramagnetic Resonance (EPR) Spectroscopy. EPR spectra were recorded on an EMX^{plus}-10/12 CW (continuous wave) spectrometer (Bruker) equipped with the Premium X-band microwave bridge (Bruker) and with a standard rectangular cavity (ER4102003ST, Bruker). For details, see section 4 of the Supporting Information.

2.5. Computational Chemistry. All calculations were performed with the Gaussian 09 code.[31] Structural optimization of all species was performed at the density functional theory (DFT) level using the global hybrid functional PBE0[32] and a double-ζ quality basis set.[33] This basis set has been used for consistency with previous calculations on related systems.[5] The convergence of structural and energetic results, regardless of the size of basis sets, namely, LANL2DZ vs triple-ζ quality 6-311G* basis set, has been checked for benchmark molecule **8** (see Tables S10-A and S10-B in section 8.2 of the Supporting Information). Solvent effects were included by means of the conductor-like polarizable continuum model (CPCM).[34] Calculations of hyperfine coupling constants were performed at the same level of theory using the purposely tailored EPR-II basis set.[35]

3. RESULTS AND DISCUSSION

Ten pyridinium-based electrophores were investigated with the emphasis on the first two ETs and their relationship to correlated (induced) structural rearrangements. All derivatives were characterized by direct current (dc) polarography, cyclic voltammetry (CV), phase-sensitive alternating current (ac) polarography, and electrochemical impedance spectroscopy (EIS) in DMSO and ACN. Selected representative compounds were characterized also by in situ EPR spectroelectrochemistry. From our previous work[5,6,17] it was expected that all

DOI: 10.1021/jacs.5b05545
J. Am. Chem. Soc. 2015, 137, 11349−11364

compounds would be reduced by at least two electrons. However, seemingly structurally similar pyridinium derivatives show two distinct types of electrochemical behavior, namely, stepwise (compounds **1**−**7**; Chart 2) and single-step (compounds **8**−**10**; Chart 2) two-electron reduction, the kinetic features of which will be described in the following sections.

The series **1**−**7** encompasses *N*-alkylpyridiniums (NAPs) **1**−**3** but also *expanded* pyridiniums (EPs) **4**−**7** (Chart 1) that are "overcongested" in the sense that their *N*-pyridinio aryl groups (Ar^1; Chart 1) are decorated with bulky methyl or phenyl substituents likely to hamper or even preclude *N*-pyramidalization and other types of distortions (Scheme 1). The dc polarograms of all seven compounds **1**−**7** are of similar shape (see Figure 1A). The slope of the log-plot analysis corresponds

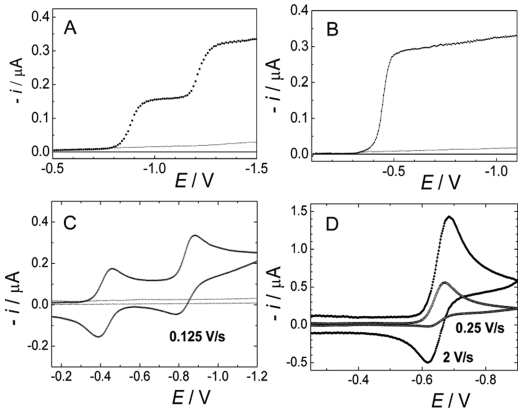

Figure 1. Direct current polarography of 0.5 mM **1** (A) and **8** (B). Cyclic voltammetry of 0.5 mM **7** (C) and **9** (D) at scan rates indicated. Samples were measured in 0.1 M $TBAPF_6$ and DMSO. Dotted lines are the supporting electrolyte alone.

to a RT/F value of 60 mV for each of the two steps, thus confirming one-electron transfers. The number (n) of electrons transferred in each step was further ascertained by comparison of the CV peak currents with the oxidation peak current of ferrocene (n = 1). Diffusion coefficients of compounds **1**−**7** were evaluated from the diffusion-limited currents of the dc polarograms. All compounds give reversible cyclic voltammograms at all scan rates investigated for the first ET (Figure 1C). It will be shown later, by impedance measurements, that the second ET is slower than the first one.

A quite different electrophoric behavior was found for compounds **8**−**10**, which are *regular* EPs in the sense that their pyridylium Ar^1 group (denoted qPy in Chart 2) is not sterically burdened. Direct current polarograms show only a single two-electron wave (Figure 1B) but cyclic voltammograms yield different patterns. For **9** and **10**, the ET has irreversible features at low scan rates (0.25 V/s), whereas on a somewhat shorter time scale (2 V/s), the ET is reversible (Figure 1D). Conversely, for **8**, the two-electron reduction process is reversible at all scan rates.

3.1. Mechanistic Issues in Question. The redox behavior of different types of pyridinium-based compounds (Charts 1 and 2), including the NAPs and EPs shown in Figure 1, draws attention to the importance of structural and charge delocalization changes on the overall pathway of two-electron uptake. These factors determine the values of standard redox potentials and their relative shifts (up to compression or inversion). However, the change of molecular structure triggered by a stepwise electron uptake is a hidden kinetic process. Such hidden transformations are probably involved to a greater or lesser extent in compounds **1**−**7**, which seemingly follow the established scheme of stepwise reductions of MV. We consider this a mechanistic issue to be solved by examining the ET rates and correlation with various optimized electromeric structures, including the intermediates and final redox products.

It is worth noting that, even though all branched EPs hitherto investigated undergo redox-triggered distortions, the actual impact of structural reorganization on ET kinetics remains unknown. Therefore, an investigation of model heavily hindered EPs **4**, **5**, and **7** (Chart 2) that are designed[36] to retain their rodlike shape during their double reduction should provide a reference point for the subsequent study of charge handling in related fluxional electrophores. Indeed, according to Marcus theory, ET rate constants contain information related to the magnitude of reorganization energy of molecular landscapes, which encompasses not only intramolecular adaptive changes (in the widest sense) but also adjustments of their direct surroundings (also referred to as "outer sphere"). On this basis, ET kinetic characteristics obtained for well-defined molecular landscapes can be viewed as a means of probing elusive steps of complicated fluxional systems.

From a methodological point of view, one can apply electrochemical methods that probe different time domains, ranging from slow methods like UV−vis−NIR spectroelectrochemistry (potential scan rates of less than 0.01 V/s), through more flexible potentiodynamic (e.g., CV) and hydrodynamic (e.g., rotating disk electrode, RDE) methods to the most universal EIS methods. In this work, we show that it is worth mapping ET kinetics of the selected compounds **1**−**10**, which constitute a library of molecular landscapes characterized by incremental variation of their inner sphere, including composition, charge, and steric hindrance (i.e., degree of freedom for their semirigid backbones). This kinetic study will be complemented with a (time-independent) computational procedure[5] aimed at identifying minima in the potential energy surfaces that describe each electrophore in its three redox states (native [Z], monoreduced [$Z - 1$], and bireduced [$Z - 2$]), with their respective structures accurately modeled at both levels of electronic and geometrical features.[5]

3.2. Setting up the Experimental Methodology of the Kinetic Study. Direct current polarographic and CV methods indicate that ETs are fast processes (Figure 1), and for this reason, the estimation of kinetic parameters requires fast methods, like the measurement of the Faradaic impedance. The cationic character, together with the semirigid polyaromatic structure of the electrophores, suggests that even in nonaqueous solvents the ET could be coupled with adsorption phenomena. Failure to detect even a subtle adsorption of redox-active species would lead to serious errors in estimation of high ET rate constants. The coupling of fast kinetics and adsorption is most conveniently investigated by phase-sensitive ac polarography and electrochemical impedance or admittance spectroscopy (EIS). Analysis of the frequency dependence of the electrode admittance Y is a rather specialized procedure, and for this reason, we describe it in section 5 of the Supporting Information.[37−42] We came to the conclusion that due to adsorption, the elucidation of kinetic parameters would be more complicated in ACN than in DMSO. The vector of the Faradaic impedance, $\mathbf{Y}_F$ (with components Y_F' and Y_F''), was

DOI: 10.1021/jacs.5b05545
J. Am. Chem. Soc. 2015, 137, 11349−11364

obtained by subtracting the double-layer capacitance from the experimental vector **Y** corrected for the solution resistance. Finally, the heterogeneous ET rate constant k^0 was evaluated from the dependence of the Faradaic phase angle φ on $\omega^{1/2}$ (ω is the angular frequency of the superimposed sine-wave voltage) according to eq 1

$$\text{cotg}\ \varphi = \frac{Y_F'}{Y_F''} = 1 + \frac{\sqrt{2D\omega}}{2k^0} \quad (1)$$

where D is the diffusion coefficient. One example of such an analysis is given in Figure 2.

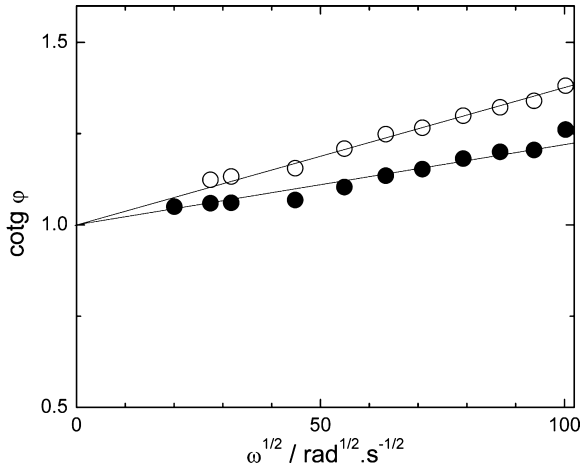

Figure 2. Dependence of the cotangent of the Faradaic phase angle φ on the applied sine-wave frequency for 1 mM **3** and 0.1 M $TBAPF_6$ in DMSO at the redox potential of the first reduction (●) and the second reduction (○). The linear regression yields the slope, from which k^0 is determined.

3.3. Case Study of the Stepwise Transfer of the First Two Electrons. Thermodynamic and kinetic data obtained for the series **1**−**7** are gathered in Table 1 (see also section 7 in the Supporting Information for comments on thermodynamic results). It should be noted that supplementary reduction processes at more negative potentials than −1.8 V were observed for almost all compounds, but these processes are beyond the scope of the present study.

As regards ET kinetics, data in Table 1 show that both the first and the second redox steps are very fast ET processes. Roughly, within the numerical uncertainty, almost all values are close to ca. 1.3 and 0.7 cm s^{-1} for k^0_1 and k^0_2, respectively. The only discrepant value is the k^0_2 rate constant of **5**, which is more than 1 order of magnitude smaller than that of other electrophores of the series (Chart 2). Also the second redox step of **6** shows some degree of quasi-reversibility (Figure S7 in the Supporting Information).

3.3.1. Insights from Combined Kinetic and Computational Analyses. Microscopic models of ET were thoroughly worked out by Marcus,[43−45] Hush,[46] Levich,[47] Dogonadze,[48] and others.[49,50] The application of Marcus theory to the ET kinetics of relatively rigid helical extended bipyridinium derivatives, "helquats", has been described recently.[51] The observation that k^0_1 is on average always higher than k^0_2 for **1**−**7** can be related to the different contributions of internal reorganization energy to ET barriers. For this series of compounds, one can assume that the previously identified redox-triggered structural change from axial to pyramidal configuration (when allowed) predominates during the second ET and is responsible for this k^0_2 lowering. However, since all members of the series show lower k^0_2 values, *the question arises as to the kind of reorganization process that becomes dominant and replaces skeletal geometry changes when these are impeded* (several EPs are indeed designed to accommodate reduction without distortion).

Molecular modeling was carried out in order to analyze the optimized geometries of each electrophore in its three redox states, including its electromers[52] (i.e., redox isomers) when they are potentially present.[5] The aim is to assess the magnitude of redox-triggered structural changes upon sequential attachment of the two electrons, concomitantly paying special attention to variations in bond-length alternation (BLA) that could reveal certain electronic structure changes, such as benzenoid-to-quinoid transitions and emerging (polarized) zwitterionic patterns. Computed molecular structures of electrophores **1**−**7** in their three redox states are displayed in Figure 3. Native geometries are all axial (see Scheme 1 and ref 5), in agreement with the single-crystal X-ray structure obtained for **5**, representative of the subclass **4**−**7** of overcongested EP electrophores (see Figure 3a).

The most significant findings derived by inspection of Figure 3 and from the analysis of the BLA (Figures 4−6) allow us to define three subclasses of electrophoric behavior on the basis of the type and extent of electronic and structural reorganization induced by the stepwise reduction.

Monocationic ([Z] = +1) electrophores of the NAP type (**1**−**3**) all show structural changes in the pyridinium core. These are mainly the bending of the methyl group out of the plane of the pyridinium ring as a result of the hybridization change of the $N_{pyridinio}$ atom. The second reduction leads to full pyramidalization accompanied by torsional relaxation of phenyl rings on either side (α-positions) of the N atom. This results in a locally flattened structure (θ_2 and $\theta_6 < 4°$; see Tables S3−S5 in the Supporting Information). As we will see throughout the present work, this type of structural relaxation, namely, the above flattening, is not only a common feature of electrophores

Table 1. Redox Potentials and the ET Rate Constants in DMSO[a]

electrophore	E^0_1/V	E^0_2/V	ΔE^0/V	k^0_1/cm s^{-1}	k^0_2/cm s^{-1}
Me-TP (**1**)	−0.883	−1.283	+0.400	1.4	0.85
Me-TP(*o*-Me) (**2**)	−0.950	−1.330	+0.380	1.3	0.83
Me-TP(*o*-Ph) (**3**)	−0.923	−1.333	+0.410	1.5	0.72
$Ph(Ph)_2$-TP (**4**)	−0.776	−1.651	+0.875	1.2	0.67
$Py(Ph)_2$-TP (**5**)	−0.655	−1.352	+0.697	0.9	0.012
$qPy(Me)_2$-TP (**6**)	−0.567	−1.004	+0.437	1.0	0.68
$qPy(Ph)_2$-TP (**7**)	−0.437	−0.845	+0.418	1.8	0.68

[a]Errors in k^0 values do not exceed 10% (see section 7 of the Supporting Information).

DOI: 10.1021/jacs.5b05545
J. Am. Chem. Soc. 2015, 137, 11349−11364

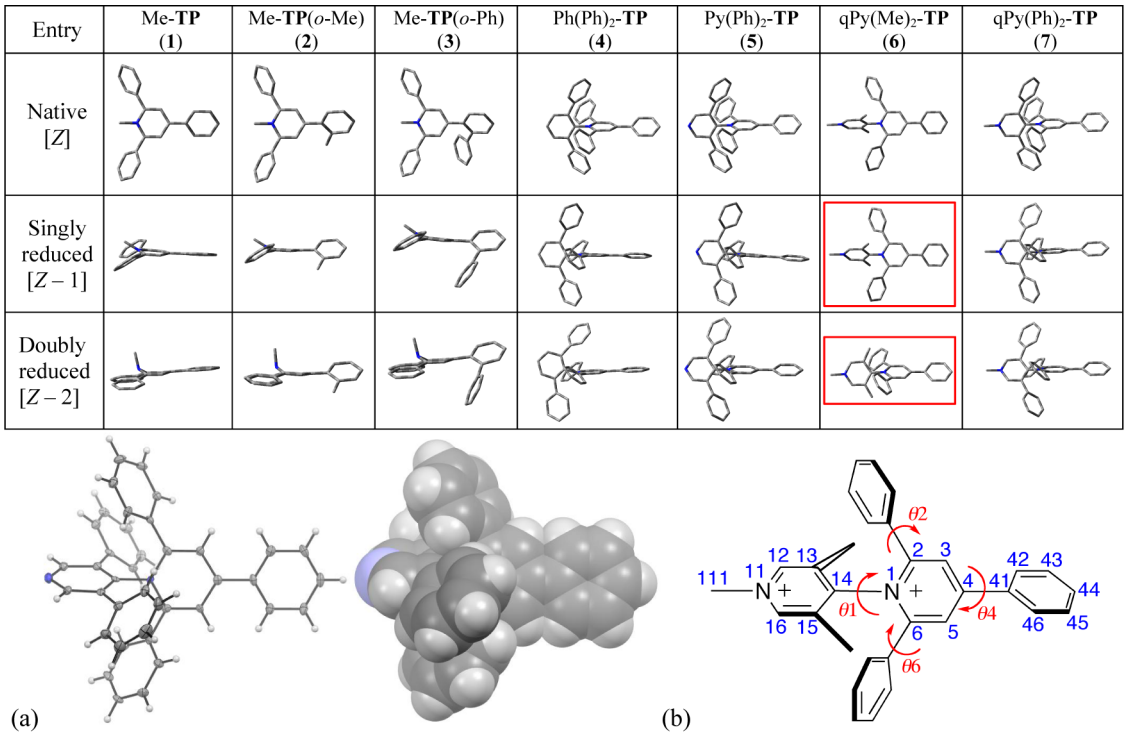

Figure 3. Structural features. Top: optimized molecular geometries of **1**−**7** in their native [Z] and singly [$Z - 1$] and doubly [$Z - 2$] reduced forms (hydrogen atoms are omitted for clarity); red framing indicates that axial and distorted electromers (AE and DE, respectively) were computed, even if only AE is represented (see section 8.1 in the Supporting Information for large-size views). Bottom: (a) single-crystal X-ray structure of congested EP **5** in its monocationic native state, illustrated as an Ortep drawing with thermal ellipsoids (50% probability) and as a van der Waals space-filling representation, and (b) numbering scheme and relevant angles in the representative case of **6**.

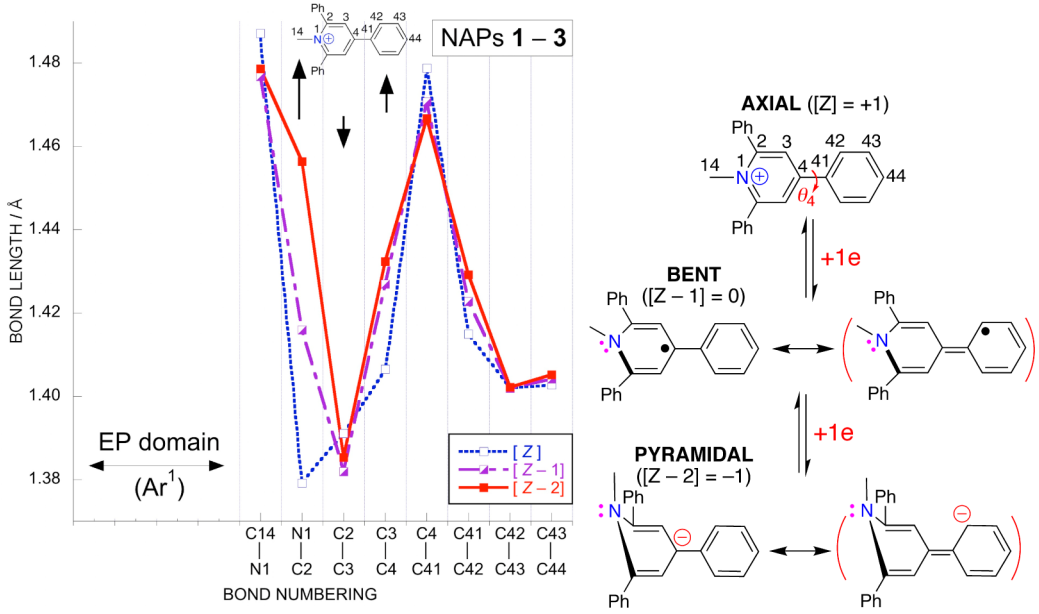

Figure 4. Bond-length plots for optimized molecular geometries[53] of **1**−**3** (average values) in their native [Z] and singly [$Z - 1$] and doubly [$Z - 2$] reduced forms, along with a formal description based on corresponding main canonical forms (minor contributions in parentheses).

that undergo a backbone distortion as adaptation to reduction but is also, in certain cases, an electrochemically noninnocent event. Overall, typical pyramidal structures resulting from these distortions feature the *N*-methyl group and the carbanion pointing toward the same side of the bireduced core platform. For this homogeneous series of NAPs, the average k^0_1 and k^0_2 values are 1.4 and 0.8 cm s^{-1}, respectively. This sizable decrease in k^0 on going from the first to the second ET is indeed consistent with a substantial structural reorganization concerted with the latter ET.

To get a more precise idea of the relative weights of steric, electronic, and electrostatic contributions to the different stages ([Z], [$Z - 1$] and [$Z - 2$]) of inner-sphere molecular reorganization, it is worth analyzing the evolution of bond

DOI: 10.1021/jacs.5b05545
J. Am. Chem. Soc. 2015, 137, 11349−11364

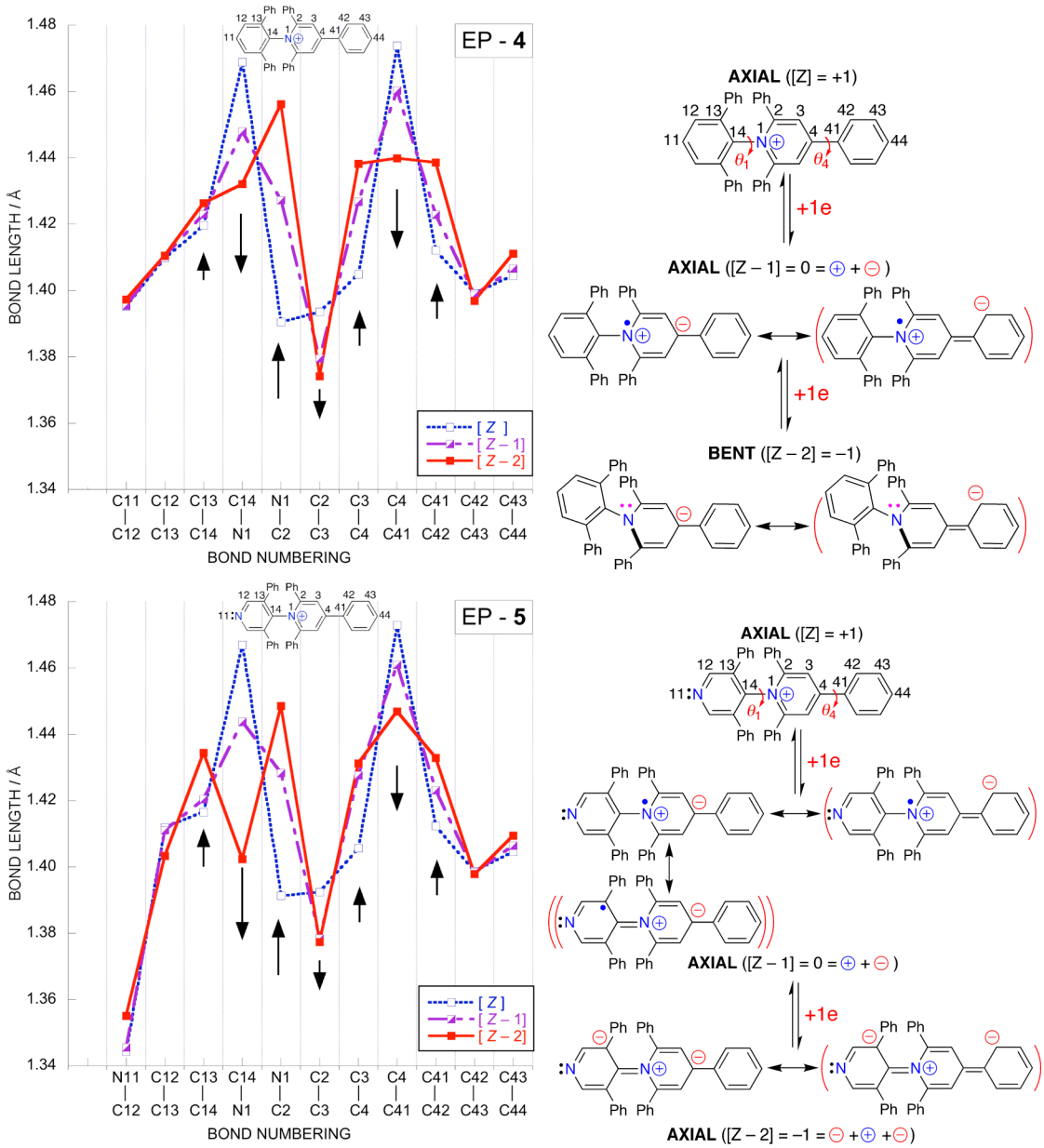

Figure 5. Bond-length plots for optimized molecular geometries[53] of **4** and **5** in their native $[Z]$ and singly $[Z-1]$ and doubly $[Z-2]$ reduced forms, along with corresponding main canonical forms.

length (BL) plots as a function of the electrophore reduction states. In the following, only BLA schemes that develop along the molecular main axis,[53] common to NAPs and EPs (Chart 1), are examined and compared.

In the case of series **1**–**3**, insofar as the BL plots are virtually superimposable despite θ_4 differences (see Figure S8-A–C in the Supporting Information), the discussion of BLA patterns is based on bond lengths that are averaged values for the three electrophores in the same redox state (Figure 4). Analysis of the BL plots tells us that the quinoid form (BLA pattern) develops on the pyridinium core and hardly extends to the terminal aryl (phenyl, tolyl, or diphenyl), which appears to be barely involved. The N1–C2 bonds of the pyridinium core are the most sensitive to reduction (elongation of ca. 0.08 Å representing ca. + 6%), all the more as they are directly involved in the distortion related to the hybridization change of N1. Thanks to the latter, the two-electron-reduced NAPs are accurately described as monoanions featuring a carbanion at the C4 site. Owing to the nature of the surrounding medium, DMSO,[54] the outer-sphere response to the incremental change of net charge is not the same for the second and the first steps: going from the neutral species ($[Z-1]=0$) to the monoanion ($[Z-2]=-1$) is more demanding from the viewpoint of solvation energy than passing from the native monocationic species ($[Z]=+1$) to the neutral form ($[Z-1]=0$), regardless of intervening distortion. Therefore, one can reasonably infer that, in addition to greater structural reorganization, the k^0 decrease ($k^0_2 \approx 0.4k^0_1$) is also related to the anionic character of the inner sphere that furthermore takes the form of a localized carbanion, thereby having a larger impact on the outer sphere than the mere cation disappearance following the first ET.

Monocationic ($[Z]=+1$) single-pyridinium-based electrophores of the EP type (**4** and **5**; Charts 1 and 2) show at the most (case of **4**) a little bending of their Ar^1 *N*-pyridinio group

DOI: 10.1021/jacs.5b05545
J. Am. Chem. Soc. 2015, 137, 11349–11364

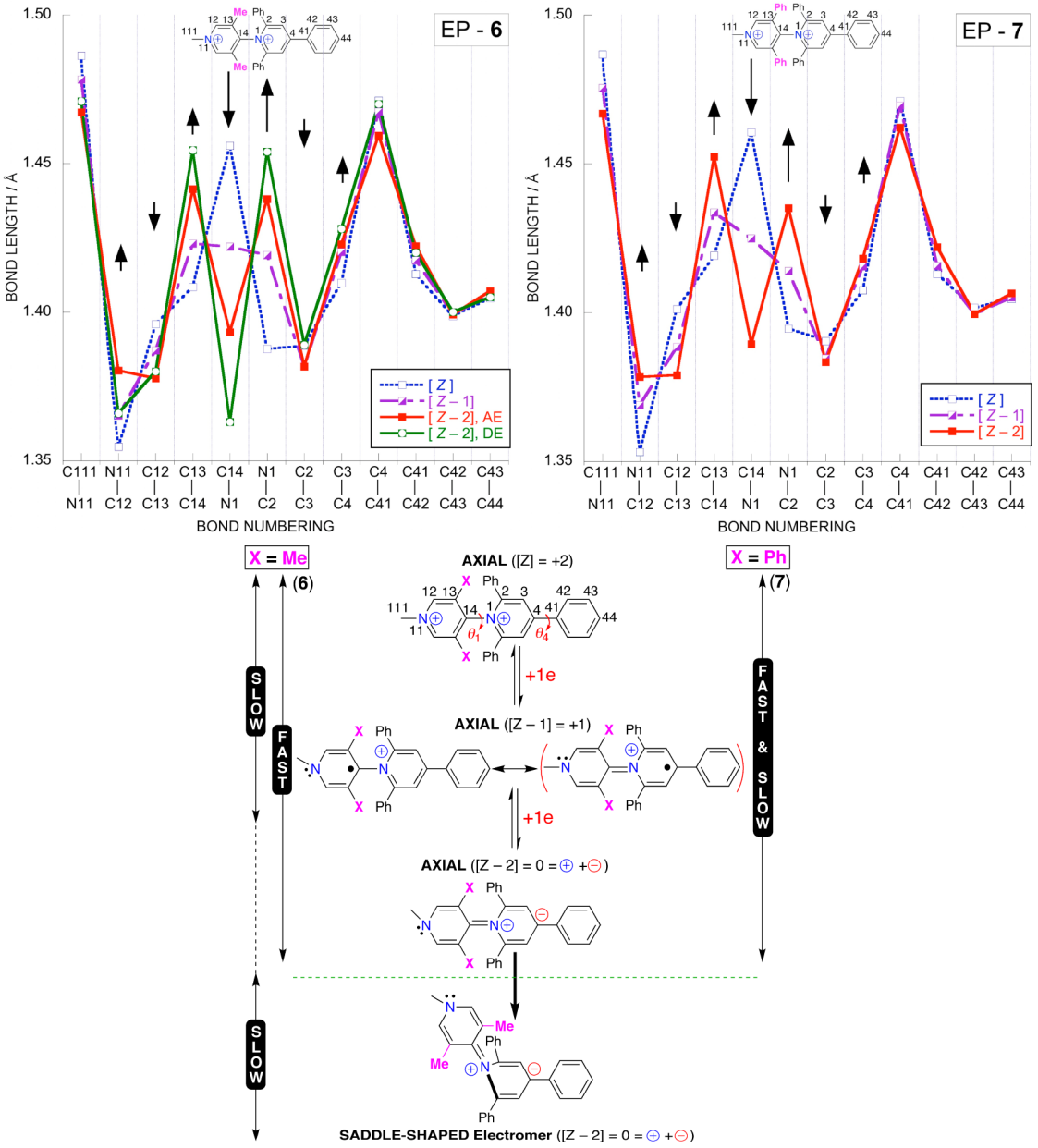

Figure 6. Bond-length plots for optimized molecular geometries[53] of **6** and **7** in their native [*Z*] and singly [*Z* − 1] and doubly [*Z* − 2] reduced forms along with corresponding main canonical forms. X = Me (for **6**) or Ph (for **7**). "Fast" and "slow" refer to the time resolution of the electrochemical study. AE and DE refer to axial and distorted electromers, respectively.

out of the mean pyridinium plane (onset of *N*-pyramidalization), which is moreover associated with the second one-electron transfer (Figure 3). Apart from this modest distortion, the main structural reorganization consists of conformational changes concerning interannular torsion angles. The more pronounced propensity to bending for **4** as compared to **5** contrasts with our previous observation[5] for related regular EPs, with sterically unencumbered *N*-pyridinio aryl groups (Ph-TP and Py-TP; i.e., X = CH and N in Scheme 1, respectively). In both cases (Ph-TP and Py-TP), a potential compression was observed (see Scheme 1)[5] that differs sharply from the situation found for **4** and **5**. Thus, we show here that bulky phenyl substituents of Ar^1 groups, in conjunction with the presence of phenyl substituents on either side of this *N*-pyridinio site of the core pyridinium, have a dramatic impact on the electro-structural reorganization of electrophores upon reduction, i.e., on reduction mechanisms. Another strong indication that the small apparent difference in structural reorganization between **4** and **5** indicates a profound difference in the way the intramolecular media handle the two electrons is clearly given by kinetic data. This discrepancy is indeed reflected in the k^0_2 rate constant that amounts to ca. 55% of k^0_1 for **4** (as is roughly the case for k^0_2 values of electrophores **1**−**3**), whereas it represents only 1.3% of k^0_1 for **5** (see Table 1).

By comparative analysis of the BL plots of **4** and **5** (Figure 5), two main findings are derived. On the one hand, upon reduction, there is a marked propensity for the quinoid structure to propagate primarily from the pyridinium core toward the terminal phenyl ring in both **4** and **5** and, second, to a lesser extent, toward the encumbered Ar^1 group when the latter is a pyridyl fragment (**5**), contrary to the case of the phenyl counterpart (**4**). This different quinoidal extension is

DOI: 10.1021/jacs.5b05545
J. Am. Chem. Soc. 2015, 137, 11349−11364

ascribed to the greater electron-withdrawing ability of the N-heterocyclic group and contributes to the stabilization of the axial geometry computed for bireduced **5**, which is not kept for **4**. In **4**, the localized shortening of the N1−C14 interannular bond is rather ascribed to a slight delocalization of the lone pair of the newly, although loosely, sp^3-hybridized $N_{pyridino}$ atom over the central phenyl of the terphenyl group [Ph(Ph)$_2$]. On the other hand, based on canonical forms, it turns out that while **4** and **5** show equivalent zwitterionic forms in their singly reduced states $[Z - 1]$, it is far from the case in their doubly reduced states $[Z - 2]$. Indeed, retention of rodlike geometry in **5** gives rise to a zwitterionic structure with formally two negative charges for a single positive charge (on the $N_{pyridinio}$ atom), while the $[Z - 2]$ of **4** is a mere monoanion. Moreover, in the case of **5**, the cationic site remains within its congested direct environment that reduces its impact on the outer sphere, so that the behavior of **5** in its $[Z - 2]$ state is best considered as that of a dianion (see Figure 5). Taking into account the properties of DMSO molecules, which clearly behave more like Lewis bases than like Lewis acids, therefore interacting preferably with cations (easy solvation),[54] it is naturally expected that such a zwitterionic pattern for the inner sphere of **5** will seriously affect the reorganization energy of the electrophoric outer sphere. Obviously, this adaptation of the surrounding medium is much more demanding and of greater extent than in the case of the two-electron-reduced **4**, in line with kinetic measurements that give k^0_2 values of 0.67 and 0.012 cm s^{-1} for **4** and **5**, respectively (Table 1).

Overall, it turns out that from the viewpoint of the impact on outer-sphere reorganization, the decreased amplitude of intramolecular structural reorganization on going from **4** to **5** is more than compensated by an increase in inner polarity, insofar as making the electrophoric skeleton more rigid is at the expense of the emergence of a zwitterionic form that promotes anionic features unsuitable to the solvation properties of the surrounding DMSO molecules.

Dicationic ($[Z]$ = +2) EPs, **6** and **7**, both keep the axial geometry of native species after the first ET and also after the second reduction in the case of **7**, like **5** (Figure 3). The situation is less clear for **6**, since two electromers (one axial and the other distorted) are computed for its $[Z - 2]$ state, as was also the case in ACN.[5] Other things being equal, the putative existence of electromers for **6**, while none is identified by theoretical exploration of **7**, is a strong indication that the methyl substituents [of the lutidylium, qPy(Me)$_2$, Ar^1 group] are sterically less efficient than the phenyl (aryl) counterparts [of the 3,5-diphenylpyridylium, qPy(Ph)$_2$, Ar^1 group] in enforcing the rodlike shape of reduced EPs. Also, electron delocalization over the two pyridinium rings connected "head-to-tail" is postulated, in spite of their geometrical decoupling (θ_1); this should contribute to the stabilization of the axial geometry of singly reduced states (see below, section 3.4). At this stage, it is worth recalling that rate constants were established using high-speed methods that correspond to a range of potential sweep rates (v) in cyclic voltammetry (i.e., $v \geq 2$ V/s), where the second ET appears as a reversible process in the cases of both **6** and **7**. For **6**, however, a loss of reversibility is observed toward the low scan-rate limit (e.g., $v \leq 0.5$ V/s),[5] while **7** shows reversible electrochemical behavior at all scan rates used (see Figure 1C).

In the special case of *closely related* electrophores **6** and **7**, which differ only in the bulky substituents of their Ar^1 groups (methyl versus phenyl), different k^0_1 values indicate that different electron-attachment sites are involved for the first ET. This finding is consistent with computational results that confirm that the different Ar^1 groups of **6** and **7** are the main support of the LUMOs of the electrophores in their native states $[Z]$ (see Chart 2 and Figures S1 and S2 in the Supporting Information).[5,6] On the other hand, identical k^0_2 values (0.68 cm s^{-1}) suggest that the pathways from $[Z - 1]$ to $[Z - 2]$ states in **6** and **7**, including inner- and outer-sphere rearrangements, are also virtually identical. With the fact in mind that only axial geometries are accessible in the case of **7**, application of the "similarity argument" allows one to infer that, of the two electromers computed for the $[Z - 2]$ state of **6**, *it is the axial species that is involved in the second ET*. It is worth recalling that in the previous study of **6**,[5] performed in ACN and relying on low-speed methods, the distorted electromer was evidenced while the axial electromer was not detected. Here it is the opposite. On the basis of these findings, it is now possible to propose sequences of BL plots along with the associated mechanistic scenarios for **6** and **7** (Figure 6).

The promotion of intramolecular charge/electronic delocalization is revealed not only by the pronounced shortening of the C14−N1 interannular bond but also by the BLA pattern, typical of a quinoid structure, that develops progressively over the *htt*-bipyridinium fragments of **6** and **7** upon reduction (Figure 6; see also section 3.3.2 below and section 9 of the Supporting Information for EPR demonstration). Overall comparative analysis of BLA schemes shows that in the case of these dicationic electrophores, the weight of the *htt*-bipyridinium motif (i.e., *N*-pyridylium-pyridinium subsystem) in the quinoid electronic delocalization process is larger than that of *N*-pyridyl-pyridinium subsystem in monocationic **5**. Furthermore, this delocalized pattern develops at the expense of quinoid extension toward C4-terminal phenyls, contrary to the situation previously observed for the monocationic species **4** and **5**.

As regards the k^0_2 value of 0.68 cm s^{-1}, common to **6** and **7**, and the use of the "similarity argument", which points to closely similar changes in molecular landscapes, mechanistic scenarios derived from analysis of BLA schemes conform to expectation. Namely, on going from the $[Z - 1]$ to the $[Z - 2]$ states, similar axial geometries and degrees of charge delocalization are involved for the inner-sphere components of **6** and **7**, which result in similar outer-sphere reorganizations.

The difference in electrochemical reversibility between low and high (potential) scan rates observed for the second reduction process of **6** (Figure S7 in the Supporting Information), together with the fact that the E^0_2 value (−1.004 V) is the same regardless of the scan rate, indicate the existence of an ET-coupled follow-up reaction ascribed to the intervention of the other (distorted) electromer in the $[Z - 2]$ state. Here, it is worth noting that the critical distortion approaching a "saddle-shaped" geometry has nothing to do with above-invoked distortions referred to as "pyramidal" or "bent" and resulting from *N*-pyramidalization in monocationic regular EPs, i.e., the hybridization change accompanying the local reduction of the $N_{pyridinio}$ atom. Indeed, in the distorted electromer of **6**, the nitrogen atom (N1) of the pyridinium core remains formally positively charged, in spite of successive reductions of the whole electrophore. For this electromeric structure, the presence of the methyl substituents of Ar^1, together with the flattening of the two phenyl rings ortho to the $N_{pyridinio}$ atom of the core platform[55] (see discussion of **1**−**3**), is likely to lock the molecular skeleton after relaxation. This

DOI: 10.1021/jacs.5b05545
J. Am. Chem. Soc. 2015, 137, 11349−11364

relaxation has time to go to completion at low scan rates but not at high scan rates, hence the observed difference in reversibility. This new assignment of the respective contributions of axial and distorted electromers of **6** allows one to clarify the mechanism of its ET process. Indeed, in our previous study,[5] the failure to detect the axial electromer when relying on low-speed analytical tools (cf. section 3.1) led to the assumption that molecular distortion was "most likely concerted with the second ET", in spite of computational indications that this axial redox isomer was more stable (see also the comment on computed energy difference between electromers in the $[Z - 2]$ state in section 8.6 of the Supporting Information). The new approach adopted in the present work allows one to reconcile the experimental and theoretical results and unambiguously shows that saddle-shaped distortion (moreover, fundamentally different from *N*-pyramidalization) is *subsequent* to the second ET (Figure 6).

The saddle-shaped configuration of the two-electron-reduced electromer (Figures 6 and 7) is the result of competing and

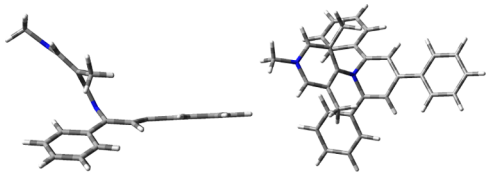

Figure 7. Optimized geometry of distorted (saddle-shaped) electromer of **6** in its $[Z - 2]$ state, side and top views.

conflicting intramolecular effects around the C14−N1 interannular bond, which are electron delocalization (embodied in the quinoidal structure) and steric hindrance. This type of severely distorted structure is not unprecedented and is somewhat reminiscent of that encountered in certain π-extended systems based on the anthryl platform derivatized at its 9 (10) position(s) with electroactive group(s), with the peri H atoms of anthracene playing the same steric role as α-phenyl rings of the pyridinium core of EPs. 9,10-Bis(1,3-dithiol-2-ylidene)-9,10-dihydroanthracene derivatives[56] as "π-extended TTFs"[57] (TTF = tetrathiafulvalene), tetracyano-9,10-anthraquinodimethane species[58] as "π-extended TCNQ"[59] (TCNQ = tetracyanoquinodimethane), or bis-quinone-anthracene[60] are such typical examples, even though distorted structures are in these cases adopted in the ground state (recovering the usual axially distorted geometry upon oxidation or reduction, respectively).[61]

To summarize this section, we have demonstrated that the combination of kinetic measurements with molecular modeling provides a powerful tool to decipher the very nature of the various mechanisms underpinning molecular-level, multielectron handling in these EPs. From a methodological viewpoint, it is, however, worth emphasizing the limit of the present phenomenological approach, based on the benchmarking of ET kinetics (viewed as the fingerprints of redox-triggered changes in molecular landscapes) in order to get insights into fluxional electrophoric functioning. Indeed, this caveat stems from the fact that direct comparison of ET rate constants is meaningful and informative *only* in the case of *closely related* electrophores, as defined on the basis of the unambiguous and precise knowledge of their characteristics, including structural degrees of freedom (provided by molecular modeling, for instance) and the extent of intramolecular charge delocalization. As exemplified by the case studies of dications **6** and **7** (k^0_2 = 0.68 cm s^{-1}) and monocation **4** (k^0_2 = 0.67 cm s^{-1}) discussed above, virtually the same rate constants for the second ET refer to different mechanisms for intramolecular charge (electron) handling, so their overall comparison is meaningless.

The picture we get by crossing the kinetic data with computational results on the molecular structures is consistent with our prime assumption, derived from the rough comparison of ET kinetics, and conforms also to our previous notion[5] concerning sterically congested EPs: the main structural and electronic relaxations occur during the second ET. Steric factors regulate not only the energetics of ET processes but also their kinetics. The impact of the emerging zwitterionic structure (due to the molecular skeleton made more rigid) replaces the impact of structural distortion on the surrounding medium, i.e., the outer-sphere component of the reorganization energy contribution to the ET kinetics. Lastly, we have shown that, depending on whether the EPs are made up of one or two (*htt*-connected) pyridinium rings, the nature of the intervening distortions (when allowed) is different: *N*-pyramidalization due to hybridization change in the former case (monocationic) versus saddle-shaped configuration resulting from the conflicting interplay of intramolecular interactions in the latter case (dicationic).

3.3.2. Introducing the Notion of "Potential Expansion". From the standpoint of ET energetics, the differentiation of related electrophores **1**−**7** relies on E^0_1 values as well as on the energy difference between the first two one-electron reduction processes ($\Delta E^0 = E^0_1 - E^0_2$). E^0_1, on the one hand, remains determined by intramolecular electronic factors,[5,6,17] as illustrated by the data of Table 1, whereas ΔE^0 depends primarily on the magnitude of structural changes triggered by electron attachment. Second, ΔE^0 for *htt*-bipyridinium derivatives and also for monocationic EPs with electron-withdrawing Ar^1 groups (like **5**) depends on both the extent and type of additional intramolecular charge delocalization effects. In other words, similar ΔE^0 values are expected for similar steric congestion around the $N_{pyridinio}$ atom, provided that the electrophores bear the same charge in their native state ($[Z]$). By involving the same number of directly linked pyridinium rings, they undergo intramolecular charge delocalization to the same extent, thereby showing similar electrostatic features. This is verified for compounds **1**−**3** ($\Delta E^0 \sim +0.4$ V in DMSO vs +0.45 V in ACN). The basic case of **1** can be taken as a reference in this respect, insofar as structural relaxation associated with sequential attachment of electrons is moreover similar to that of a mere *N*-methylpyridinium. In the case of **4**, where the *N*-pyridinio group is a bulky terphenyl moiety, a markedly larger ΔE^0 value is found (+0.875 V), which reflects the effective blocking of the hybridization change (i.e., *N*-pyramidalization). This doubling of the ΔE^0 value as compared to the reference value of +0.4 V can be attributed to the energetic penalty that originates in the electrostructural "frustration" of the $N_{pyridino}$ atom (normally sp^3-hybridized with pyramidal geometry), which is here forced to adopt an inappropriate almost planar geometry, close to that of the starting $N_{pyridinio}$ atom (sp^2-hybridized). Accordingly, the intermediate ΔE^0 value for **5** (+0.697 V) is indicative of an energy destabilization less pronounced than in **4**, which is consistent with both the proper geometry allowed for the $N_{pyridinio}$ atom, which does not change its degree of oxidation (it remains an iminium fragment), and the contribution of energy-stabilizing charge/electron delocalization, which extends to the

DOI: 10.1021/jacs.5b05545
J. Am. Chem. Soc. 2015, 137, 11349−11364

pyridyl fragment of the Ar^1 group upon reduction (see Figure 5). In spite of these favorable contributions, it remains nonetheless that the zwitterionic structure with the negatively charged pyridyl fragment is energy-demanding. Moreover, this emerging highly polarized structure is a noninnocent intramolecular adaptation to two-electron reduction, which heavily impacts on the surrounding medium; hence, the ΔE^0 value is significantly greater than +0.4 V. Thus, based on the different types of inner-sphere reorganization found for different levels of crowding (comparison of **4** and **5**), it appears that there is a kind of steric gating of the relaxation pathways that determines the type of intramolecular charge/electron-handling mode.[62] Taking the unconstrained (freely relaxing) electrophore **1** as the reference, one can introduce the notion of "expansion of the standard potentials". This is illustrated by the cases of **4** and **5**, where intramolecular steric hindrance severely constrains the structures and precludes, to various extents, skeletal relaxation (here *N*-pyramidalization). This "potential expansion" is viewed as the opposite of the "compression of standard potentials" that features ΔE^0 values thus ranging from ca. + 0.4 to 0 V for the type of electrophores studied in the present work and given the same experimental conditions,[20] including solvent and supporting electrolyte (here DMSO and $TBAPF_6$). For instance, for Me-TP, Ph-TP, and Py-TP in 0.1 M $TBAPF_6$ and ACN, ΔE^0 = +0.46, +0.16, and 0.0 V, respectively.[5] For the dicationic electrophores **6** and **7**, which show similar ΔE^0 values (+0.43 V on the average), it is worth noting that this value is closer to the above reference value (+0.4 V) than to values found for the similarly congested but monocationic electrophores **4** and **5**. The explanation of this *apparent* discrepancy is 3-fold: (i) the LUMOs of **6** and **7** in their native forms are essentially located on their pyridinium-based Ar^1 groups, which are therefore the sites for the attachment of the first electron[5] (see Chart 2 and Figure S1 in the Supporting Information); (ii) even if these pendant pyridinium fragments are bulky, their $N_{pyridinio}$ atoms (and their immediate environment) are not sterically hindered or shielded; and (iii) the extension of the LUMO over the core pyridinium ring allows electron/charge delocalization along the main axis of the electrophores, which stabilizes an axial molecular geometry for the monoreduced species, akin to that of the native species (provided there are some changes in the dihedral angles). This is reflected by the rodlike (axial) geometries computed for singly reduced forms of **6** and **7**, which are also conserved in their $[Z - 2]$ states (Figures 3 and 6). In other words, comparison of ΔE^0 with the reference value of +0.4 V is not relevant, again highlighting the fact that one has to make the distinction between single- and two-pyridinium electrophores. In fact, the electrochemical behavior of overcongested **6** and **7** is rather akin to that of MV, that is, a dicationic electrophore made of two pyridinium rings connected "tail-to-tail" (Chart 1).

In order to substantiate charge delocalization within singly reduced overcongested dicationic EPs, a complementary in situ EPR spectroelectrochemical study was undertaken to characterize the radicals of **1** (reference single-pyridinium molecule) and **6** (see the Supporting Information, Figures S9–S11 and simulation details therein). The hyperfine coupling constant (HFCC) values, which provide the best fit of the experimental EPR spectra, together with the *g*-factors (g = 2.0027 for the radical of **1** and *g* = 2.0029 for the radical cation of **6**), confirm that the spin density (or unpaired electron) is primarily delocalized over the central part of the molecule, that is, over the pyridinium core for **1** and the "head-to-tail" bipyridinium subsystem in the case of **6** (see Figures S2 and S3 in the Supporting Information). The HFCC values of radical cation of **6** are accordingly smaller than those of **1**.

To summarize, ΔE^0 values of mono- and dicationic species are not directly comparable, even less so when the axial geometry is sterically maintained, thereby further promoting the interplay between Ar^1 (when electroactive) and the pyridinium core, i.e., inter-pyridinium-site interaction in the case of dicationic EPs. This interplay takes the form of charge delocalization in the $[Z — 1]$ state and of an extended, although twisted, π-electron system (showing zwitterionic character) in the $[Z - 2]$ state. This delocalization explains why the number of attached electrons (in the usual potential window ranging from ca. −1.8 to 0.0 V vs SCE) is to a large extent independent of the number of pyridinium units forming the overall electrophoric assembly, as was already observed for MV.

Also of special interest is the striking capability of the adjustable intramolecular steric hindrance to regulate electrophoric functioning, that is, to promote specific mechanisms of electrostructural relaxation that eventually impact ΔE^0 values. One such striking example is the case of Py-TP/$Py(Ph)_2$-TP, with switching from ΔE^0 = 0 (coalescence of standard potentials that actually corresponds to the limiting case of a potential compression following *N*-pyramidalization)[5] to ΔE^0 = +0.697 V, which corresponds conversely to a "potential expansion" resulting from the strict blocking of *N*-pyramidalization.

3.4. Case Study of the Single-Step Transfer of the First Two Electrons. If electrophores **8**–**10** can be classified as *regular* EPs with respect to the low steric hindrance of their pyridylium Ar^1 group (denoted qPy in Chart 2), they nonetheless show varied levels of congestion about their core pyridiniums. Indeed, H atoms at the β-position (Chart 1) in the former TP series (**4**–**7**) plus **8** are replaced by methyl and phenyl groups to give EPs of the DMTP (**9**) and XP (**10**) types, respectively. These EPs have similar redox characteristics and accept two electrons, like **1**–**7** derivatives, however, in an apparent single step[5] (experimentally, ΔE^0 = 0 V). This is seen, for instance, in the single dc polarographic wave of **8**–**10**, with the limiting current being twice as high as that for the first wave of compound **1** at the same concentration (Figure 1B). As is the case for the series **1**–**7**, (i) E^0_1 (or $E_{1/2}$) values are essentially determined by the intramolecular electronic effect of the various substituents, that is, here, by the β-substituent only (H, Me, or Ph), and (ii) ΔE^0 values are largely governed by the magnitude of structural reorganization, which is large for the **8**–**10** series;[5] hence, the *apparent* ΔE^0 = 0 V.

In order to obtain the individual values of E^0_1 and E^0_2, we performed the log-plot analysis [i.e., $\log(i/(i_{lim} - i)$ against E, where i is the current at E and i_{lim} is the limiting current] of the polarographic data (Figure 8). Indeed, this plot shows two clearly defined linear slopes at the lowest and highest potentials, both limits having slopes corresponding to a single ET. The extrapolated intercepts with the potential axis can be considered as estimates of the individual formal redox potentials corresponding to each elementary ET. Thus, it is found that the second standard redox potential (E^0_2) is more positive than the first (E^0_1), which confirms that the single-step two-electron reduction observed for **8**–**10** originates in a "potential inversion" phenomenon. For all three electrophores, the calculated difference between the derived E^0 values (ΔE^0 =

DOI: 10.1021/jacs.5b05545
J. Am. Chem. Soc. 2015, 137, 11349–11364

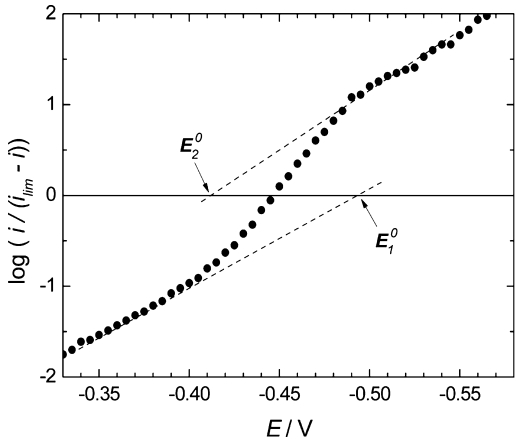

Figure 8. Log-plot analysis of a polarographic wave of **8** in DMSO given in Figure 1B. Arrows indicate estimated first and second redox potentials.

$E^0_1 - E^0_2$) is therefore negative by ca. −0.1 V on average. Data are summarized in Table 2.

Table 2. Redox Potentials and Rate Constants Determined in DMSO[a]

electrophore	$E_{1/2}$/V	E^0_1/V	E^0_2/V	ΔE^0/V	k^0/cm s^{-1}
qPy-TP (**8**)	−0.444	−0.495	−0.410	−0.085	0.23
qPy-DMTP (**9**)	−0.642	−0.675	−0.585	−0.090	0.10
qPy-XP (**10**)	−0.528	−0.570	−0.405	−0.165	0.58

[a] $E_{1/2}$ coincides with the admittance maxima (E_Y^{max}) at low applied frequencies (two-electron process). E^0 potential values are estimated from the log-plot analysis of two-electron processes. Heterogeneous rate constants, k^0, are given for the potential of the admittance maxima.

Cyclic voltammetry reveals the following difference between these three electrophores: while compound **8** gives a reversible pair of redox peaks (E_{pc} and E_{pa}) at all scan rates from 0.06 to 2 V/s, this is not the case for compounds **9** and **10**, which show irreversibility at low scan rates (<0.5 V/s; Figure 1D) and full reversibility at higher scan rates (2 V/s and higher). Such behavior indicates the presence of a non-Faradaic process coupled with the two-electron reduction.

Heterogeneous ET rate constants (k^0) of electrophores **8**−**10** were obtained using ac polarography, and each k^0 refers to the rate of the rate-determining step, i.e., the smaller rate of the two ETs. The observation of a single-step two-electron reduction usually implies that the first ET is the rate-determining step. The fact that the rate constants for this series of electrophores are lower than for **1**−**7** allowed their evaluation from ac polarograms in DMSO at 160 Hz, which show one simple sharp peak on both admittance components, with no indication of adsorption (see Figure S5 in the Supporting Information along with discussion on reactant adsorption). The ac polarograms were corrected for the solution resistance (R_s) by vectorial subtraction, and the ET rate constants [$k(E)$] were evaluated as a function of the dc potential (E), yielding the k^0 rate constants. An example of the estimation of k^0 from the ac polarogram along with the plot of $k(E)$ vs E (eq 2) is given in Figure 9.

$$k(E) = \frac{Y_F''(E)}{Y_F'(E) - Y_F''(E)}\sqrt{2\omega D} \qquad (2)$$

The rate constants k^0, given by the intersection of the two linear asymptotes, are listed in Table 2.

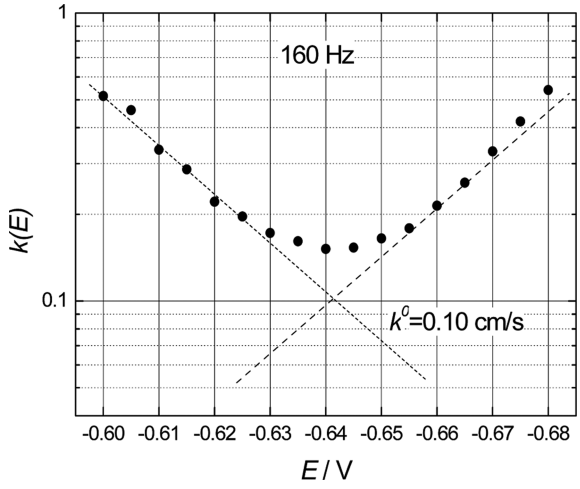

Figure 9. Dependence of the ET rate constant, k, on the potential for **9** in DMSO. Data were evaluated from the ac polarograms measured at 160 Hz.

From a mechanistic viewpoint, the transfer of the first electron, together with a subsequent structural change similar to that depicted in Scheme 1 (although different in nature, see below) that prepares the second ET, is constitutive of the rate-determining step of the overall process. In our previous study,[5] devoted to energetic aspects of ET processes in these three electrophores (among others), a key role was assigned to electromers of singly reduced species and their equilibria in the achievement of the net two-electron processes. Overall, the axial/distorted interconversion between one-electron-reduced electromers was assumed to prepare the severely distorted electrophoric structures computed for bireduced products. In such a situation, the second electron transfer is energetically and kinetically facilitated, which leads us to observe a "single two-electron reduction wave" ascribed to "potential inversion".

At this stage, analysis of the BL plots derived from optimized geometries of **8**−**10** in DMSO provides valuable mechanistic insights into electrophoric functioning (Figure 10). The most salient feature stems from the continuous development of the quinoidal form parallel to the reduction level that, this time, is driven to completion. The key role of axial and distorted electromers in the [Z − 1] state, already invoked in the previous study in ACN,[5] is further confirmed in DMSO. The [Z − 1] distorted electromer (DE), featuring the onset of a saddle-shaped structure, is here found to be isoenergetic with the axial electromer (AE) within the precision of the theoretical method in the case of **8** (within 0.015 kcal mol^{-1}) and *almost* isoenergetic in the case of **10** (AE is more stable than DE by 1.8 kcal mol^{-1}). Note that, contrary to the axial electromer of the less strained EP **8**, axial forms/electromers of congested EPs (**4**−**7**, **9**, **10**) in their [Z − 1] states do not exhibit marked BLA features around their Ar^1/core pyridinium interannular region that encompasses the C13−C14, C14−N1, and N1−C2 bonds (compare the [Z − 1] BL plots of Figures 5, 6, and 10). The different levels of steric constraint around the pyridinium cores are also reflected by BL variations upon successive reductions for **10**, which are of larger amplitude than in the case of **8** (Figure 10). In the [Z − 2] state, the fully developed saddle-shaped electromer is computed to be by far more stable than its

DOI: 10.1021/jacs.5b05545
J. Am. Chem. Soc. 2015, 137, 11349−11364

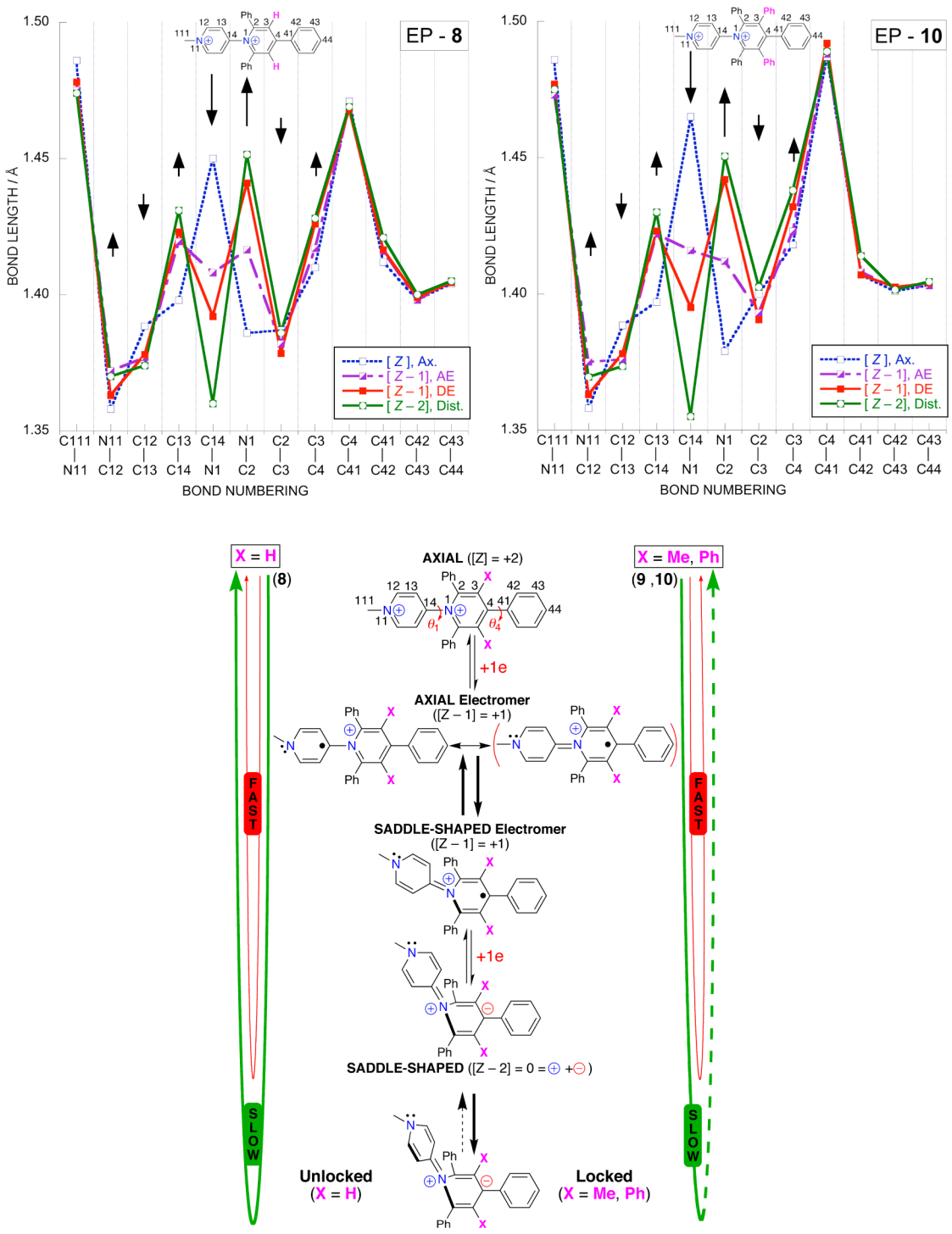

Figure 10. Top: Bond-length plots for optimized molecular geometries[53] of **8** and **10** in their native [*Z*] and singly [*Z* − 1] and doubly [*Z* − 2] reduced forms; AE and DE refer to axial and distorted electromers, respectively. Bottom: corresponding main canonical forms, with X = H (for **8**), Me (for **9**), or Ph (for **10**). "Fast" and "slow" refer to scan rate in CV, with the dotted arrow representing the loss of reversibility (no reoxidation wave).

axial counterpart in the three cases of **8**−**10**, so that AE is not considered in the electrophoric mechanism. The bending of the Ar^1 group (qPy) gives rise to a saddle-shaped distortion that is reversible at high scan rates, but further relaxation of this ring, such as its twisting, is likely to lock the structure of the most β-congested EPs, thereby explaining the loss of electrochemical reversibility observed for **9** and **10** at low scan rates (Figure 10). This "locking process" is traced back to the β substituent via an indirect steric effect mediated by the α-phenyl rings of the $N_{pyridinio}$ atom. Once again, it involves the flattening of these α-rings (represented by torsion angles θ_2 and θ_6; Figure 3b) concomitantly with torsional relaxation about θ_1 (see Tables S10−S12 in the Supporting Information).

To further support the relevance of this mechanistic scenario, EPR investigations were undertaken. The typical EPR spectra of the radical cations of **8** and **9** exhibit broad lines (ΔB_{pp} = 1.2

DOI: 10.1021/jacs.5b05545
J. Am. Chem. Soc. 2015, 137, 11349−11364

mT) without any hyperfine structure and very low intensity (Figure S12 in the Supporting Information). This is evidenced by comparison with spectra of **1** and **6**, after all spectra were normalized with respect to (i) the EPR Q-factor, (ii) the number of scans, and (iii) the concentration of the starting compounds. These findings support one-electron reduction in the case of **1** and **6** and two-electron reduction for **8** and **9**. The very low concentration of the radical cations is consistent with the values of the disproportionation constant, K_{disp}, obtained from $(E^0_2 - E^0_1)$ differences: 27 for compound **8**, 33 for **9**, and 625 for **10**, respectively. Besides, and most importantly, detection of traces of intermediate one-electron-reduced species (from disproportionation equilibria) de facto indicates that these potential inversion processes *are not* concerted two-electron transfers, as was also anticipated from the moderately negative values (i.e., >−0.4 V) of ΔE^0.[20] Thus, the overall picture we get fully conforms to the single-step two-electron transfer mechanism proposed in Figure 10.

4. CONCLUSIONS

The particular electrochemical sensitivity of the α-, γ-aryl-substituted pyridinium platform to the steric and electronic features of its aryl *N*-group (Ar^1) justifies that the so-called EPs, for "*N*-aryl-expanded pyridiniums", should be considered as forming a specific class of electrophores in its own right. From the viewpoint of molecular design, it is worth emphasizing the intrinsic dissymmetry of electrophoric systems, whether stemming from the very nature of EPs or from the "*head-to-tail*" connection scheme of bipyridinium assemblies. This vectorial feature is of critical importance in the unique electrochemical flexibility that characterizes this class of electrophores (ranging from "potential expansion" to "potential inversion") that, thereby, can undergo fast to ultrafast ETs in a controllable manner (i.e., from stepwise to single-step two-electron transfer). Within this framework, we have demonstrated the pivotal role of intramolecular steric hindrance that functions as an adjustable parameter to effectively regulate the rich electrophoric activity of EPs, including the energetics (standard potentials, E^0) and the kinetics (heterogeneous rate constants, k^0) of ETs.

When the EPs *are not* overcongested around their Ar^1–$N_{pyridinio}$ interannular linkage (i.e., C14–N1), they can undergo two distinct types of redox-triggered distortion that hitherto were both loosely referred to as the same "*N*-pyramidalization", due to their apparent overall similarity. The nature of these distortions, as electrostructural relaxation pathways, depends on the number (n = 1 or 2) of constitutive pyridinium rings (provided that there is a "head-to-tail" connection scheme when n = 2). For the single-pyridinium electrophores, a genuine *N*-pyramidalization associated with the hybridization change of the locally reduced $N_{pyridinio}$ atom occurs, following the EP reduction. For the dicationic *htt*-bipyridinium electrophores, it is a saddle-shaped skeletal distortion resulting from conflicting intramolecular interactions (i.e., electronic delocalization versus steric hindrance) that occurs. If *N*-pyramidalization within single-pyridinium EPs was found to be associated with a *compression* of standard potentials, the saddle-shaped distortion within *htt*-bipyridinium EPs was found to be associated with an *inversion* of standard potentials. In both cases, the reversibility of ET processes is then correlated with ancillary steric constraints and relaxation processes, referred to as "locking processes". To what extent *N*-pyramidalization could also be involved in "potential inversion" and the saddle-shaped distortion be related to "potential compression" remain to be clarified.

When the EPs *are* overcongested around their Ar^1–$N_{pyridinio}$ interannular linkage, the enforced slightly bent or even rodlike (i.e., axial) skeletal geometry generates an electrostructural "frustration" (**4**) and/or the promotion of a polarized zwitterionic arrangement (**5**). For such encumbered single-pyridinium EPs, these energy-demanding ways of adaptating to two-electron reduction lead to further separate the standard potentials as compared to the potential separation of *N*-methyl-2,4,6-triphenylpyridinium (**1**), taken as a reference electrophore. This phenomenon, defined as the opposite of "potential compression", is here referred to as "potential *expansion*". More generally, stepwise two-electron reduction of sterically overcongested EPs, and especially of *htt*-bipyridinium derivatives, gives rise to a charge delocalization in the $[Z - 1]$ state along with electron delocalization (extended π-conjugated system taking the quinoidal form) that propagate from the pyridinium core to the electroactive Ar^1 group (and/or vice versa) in spite of geometrical decoupling (represented by θ_1). The N1–C14 interannular bond continuously shortens as the torsion angle θ_1 decreases, with its double-bond character increasing upon reduction, as a bent bond (also called "banana bond") progressively builds up, giving rise to the twisted π-electron system of the electrophores reduced to their $[Z - 2]$ state. The picture we get of the electrochemical behavior of such overcongested aryl-expanded *htt*-bipyridiniums is therefore reminiscent of that of "tail-to-tail" bipyridinium, that is to say, prototypical MV, as a representative of redox systems of the Weitz type.

Experimental rate constants (represented by k^0 values) indicate the most prominent mechanistic aspects for reduction of pyridinium-based electrophores **1**–**10** and serve to gain valuable insights into the complex electrophoric behaviors investigated. For the series of molecules **1**–**7**, the second ET process is always slower than the first one (main structural changes and/or solvent reorganization associated with the second ET), whereas the rate constants for the single-step two-electron reduction of **8**–**10** are even smaller and indicate the main changes upon the first ET.

Overall, in the light of the valuable insights we have gained into the manner by which EP electrophoric entities handle multielectron uptake/release, it becomes easier to embark upon molecular design.[63] In particular, better-informed decisions can now be taken on the wisest utilization for the various forms of EPs as a function of specific requirements attached to target implementations, spanning from catalysis to redox-switchable twisted molecular π-chromophores or "TICTOID" NLO-phores,[64] for instance.

■ ASSOCIATED CONTENT

Supporting Information

The Supporting Information is available free of charge on the ACS Publications website at DOI: 10.1021/jacs.5b05545.

Complete refs 4 and 31; computational results for **1**–**10**, including relevant molecular orbitals (LUMOs and SOMOs) and spin densities; crystallographic data of **5**; details on electrochemical experiments and in situ EPR spectroelectrochemistry; detection of adsorption of reactants from impedance data; reversibility issues and comparison of voltammograms of **6** and **7**; comments on kinetic data precision and on correlation of thermody-

DOI: 10.1021/jacs.5b05545
J. Am. Chem. Soc. 2015, 137, 11349–11364

namic and structural properties; optimized structural features in different redox states (tables of bond lengths and angles); benchmarking of triple-ζ basis set (6-311G*) on electrophore **8** (Table S10-B and associated computed Cartesian coordinates); EPR spectra of compounds **1**, **6**, **8**, and **9** (experiment and simulation); experimental details on the synthesis and characterization of new compounds and precursors including ^{1}H NMR (400 MHz) and ^{13}C NMR (100 MHz) spectra as well as ESI mass spectra (PDF)

X-ray crystallographic data for [**5**](BF$_4$) in CIF format (CIF)

AUTHOR INFORMATION

Corresponding Authors

*ilaria.ciofini@chimie-paristech.fr

*hromadom@jh-inst.cas.cz

*lubomir.pospisil@jh-inst.cas.cz

*philippe.laine@univ-paris-diderot.fr

Notes

The authors declare no competing financial interest.

ACKNOWLEDGMENTS

Financial support by the Grant Agency of the Czech Republic (13-19213S and 14-05180S), Grant Agency of the Academy of Sciences of the Czech Republic (M200401202, RVO: 61388955), the Ministry of Education of the Czech Republic (Barrande project 7AMB15FR027), the French Ministries of Foreign Affairs (MAE) and of Education and Research (MESR) (PHC Barrande, 2015 project No. 34012SC), and the French National Research Agency, ANR (E-StorIc project: ANR-14-CE05-0002), is gratefully acknowledged. We thank Dr. J. Lomas and Dr. H.-P. Jacquot de Rouville for fruitful discussions.

REFERENCES

(1) Gebicki, J.; Marcinek, A.; Zielonka, J. *Acc. Chem. Res.* **2004**, *37*, 379.

(2) Hagfeldt, A.; Boschloo, G.; Sun, L.; Kloo, L.; Pettersson, H. *Chem. Rev.* **2010**, *110*, 6595.

(3) (a) Hammarström, L. *Acc. Chem. Res.* **2015**, *48*, 840. (b) Dyar, S. M.; Barnes, J. C.; Juríček, M.; Stoddart, J. F.; Co, D. T.; Young, R. M.; Wasielewski, M. R. *Angew. Chem., Int. Ed.* **2014**, *53*, 5371. (c) Konduri, R.; Ye, H.; MacDonnell, F. M.; Serroni, S.; Campagna, S.; Rajeshwar, K. *Angew. Chem., Int. Ed.* **2002**, *41*, 3185. (d) Gust, D.; Moore, T. A.; Moore, A. L. *Acc. Chem. Res.* **1993**, *26*, 198. (e) Wasielewski, M. R. *Chem. Rev.* **1992**, *92*, 435.

(4) Adams, D. A.; et al. *J. Phys. Chem. B* **2003**, *107*, 6668 and references therein.

(5) Fortage, J.; Peltier, C.; Perruchot, C.; Takemoto, Y.; Teki, Y.; Bedioui, F.; Marvaud, V.; Dupeyre, G.; Pospíšil, L.; Adamo, C.; Hromadová, M.; Ciofini, I.; Lainé, P. P. *J. Am. Chem. Soc.* **2012**, *134*, 2691.

(6) Fortage, J.; Peltier, C.; Nastasi, F.; Puntoriero, F.; Tuyèras, F.; Griveau, S.; Bedioui, F.; Adamo, C.; Ciofini, I.; Campagna, S.; Lainé, P. P. *J. Am. Chem. Soc.* **2010**, *132*, 16700.

(7) Volke, J.; Naarová, M. *Collect. Czech. Chem. Commun.* **1972**, *37*, 3361.

(8) Mc Namara, F. T.; Nieft, J. W.; Ambrose, J. F.; Huyser, E. S. *J. Org. Chem.* **1977**, *42*, 988.

(9) Raghavan, R.; Iwamoto, R. T. *J. Electroanal. Chem. Interfacial Electrochem.* **1979**, *102*, 85.

(10) Carelli, I.; Cardinali, M. E.; Micheletti Moracci, F. *J. Electroanal. Chem. Interfacial Electrochem.* **1980**, *107*, 391.

(11) Kinoshita, H.; Uehara, M.; Nakaya, J.-I. *Bull. Univ. Osaka Prefect., Ser. A* **1981**, *29*, 157.

(12) Hromadová, M.; Pospíšil, L.; Sokolová, R.; Kolivoška, V. *Collect. Czech. Chem. Commun.* **2011**, *76*, 1895.

(13) *The Viologens. Physicochemical Properties, Synthesis and Applications of the Salts of 4,4′-Bipyridine*; Monk, P. M. S., Ed.; John Wiley & Sons: Chichester, U.K., 1998.

(14) Volke, J.; Urban, J.; Volkeová, V. *Electrochim. Acta* **1994**, *39*, 2049.

(15) Volke, J.; Dunsch, L.; Volkeova, V.; Petr, A.; Urban, J. *Electrochim. Acta* **1997**, *42*, 1771.

(16) (a) Katritzky, A. R.; Marson, C. *Angew. Chem., Int. Ed. Engl.* **1984**, *23*, 420. (b) Katritzky, A. R. *Tetrahedron* **1980**, *36*, 679.

(17) Fortage, J.; Tuyèras, F.; Ochsenbein, P.; Puntoriero, F.; Nastasi, F.; Campagna, S.; Griveau, S.; Bedioui, F.; Ciofini, I.; Lainé, P. P. *Chem. - Eur. J.* **2010**, *16*, 11047.

(18) Peltier, C.; Adamo, C.; Lainé, P. P.; Campagna, S.; Puntoriero, F.; Ciofini, I. *J. Phys. Chem. A* **2010**, *114*, 8434.

(19) Hünig, S.; Berneth, H. *Top. Curr. Chem.* **1980**, *92*, 1.

(20) Evans, D. H. *Chem. Rev.* **2008**, *108*, 2113 and references therein.

(21) The most popular pyridinium-based electron mediators (or relays) are arguably bipyridinium derivatives and, in particular, methyl viologen: (a) ref 19. (b) Bird, C. L.; Kuhn, A. T. *Chem. Soc. Rev.* **1981**, *10*, 49. As an electron mediator, MV significantly contributed to the launching and development of "artificial photosynthesis", e.g., in multimolecular systems for hydrogen evolution: (c) Lehn, J.-M.; Sauvage, J.-P. *Nouv. J. Chim.* **1977**, *1*, 449. (d) Moradpour, A.; Amouyal, E.; Keller, P.; Kagan, H. *Nouv. J. Chim.* **1978**, *2*, 547. (e) Kalyanasundaram, K.; Kiwi, J.; Grätzel, M. *Helv. Chim. Acta* **1978**, *61*, 2720. (f) Harriman, A.; Porter, G. *J. Chem. Soc., Faraday Trans. 2* **1982**, *78*, 1937. There exist also single-pyridinium and multi-pyridinium mediators; see, for instance, the following: (g) Matsuo, T.; Asano, A.; Ando, T.; Hisaeda, Y.; Hayashi, T. *Chem. Commun.* **2008**, 3684. (h) Neumann-Spallart, M.; Bauer, R. *Mater. Express* **2011**, *1*, 350.

(22) For the catalytic reduction of CO_2, as a benchmark example, see the following: (a) Lim, C.-H.; Holder, A. M.; Hynes, J. T.; Musgrave, C. B. *J. Am. Chem. Soc.* **2014**, *136*, 16081. (b) Barton Cole, E.; Lakkaraju, P. S.; Rampulla, D. M.; Morris, A. J.; Abelev, E.; Bocarsly, A. B. *J. Am. Chem. Soc.* **2010**, *132*, 11539. (c) Barton, E. E.; Rampulla, D. M.; Bocarsly, A. B. *J. Am. Chem. Soc.* **2008**, *130*, 6342.

(23) Reichardt, C. *Chem. Soc. Rev.* **1992**, *21*, 147.

(24) (a) Coe, B. J.; Harris, J. A.; Asselberghs, I.; Wostyn, K.; Clays, K.; Persoons, A.; Brunschwig, B. S.; Coles, S. J.; Gelbrich, T.; Light, M. E.; Hursthouse, M. B.; Nakatani, K. *Adv. Funct. Mater.* **2003**, *13*, 347. (b) Konstantaki, M.; Koudoumas, E.; Couris, S.; Lainé, P.; Amouyal, E.; Leach, S. *J. Phys. Chem. B* **2001**, *105*, 10797.

(25) (a) Lainé, P. P.; Campagna, S.; Loiseau, F. *Coord. Chem. Rev.* **2008**, *252*, 2552. (b) Lainé, P.; Amouyal, E. *Chem. Commun.* **1999**, 935.

(26) (a) Fortage, J.; Dupeyre, G.; Tuyèras, F.; Marvaud, V.; Ochsenbein, P.; Ciofini, I.; Hromadová, M.; Pospíšil, L.; Arrigo, A.; Trovato, E.; Puntoriero, F.; Lainé, P. P.; Campagna, S. *Inorg. Chem.* **2013**, *52*, 11944. (b) Fortage, J.; Puntoriero, F.; Tuyèras, F.; Dupeyre, G.; Arrigo, A.; Ciofini, I.; Lainé, P. P.; Campagna, S. *Inorg. Chem.* **2012**, *51*, 5342. (c) Fortage, J.; Tuyèras, F.; Peltier, C.; Dupeyre, G.; Calboréan, A.; Bedioui, F.; Ochsenbein, P.; Puntoriero, F.; Campagna, S.; Ciofini, I.; Lainé, P. P. *J. Phys. Chem. A* **2012**, *116*, 7880.

(27) Kolivoška, V.; Gál, M.; Pospíšil, L.; Valášek, M.; Hromadová, M. *Phys. Chem. Chem. Phys.* **2011**, *13*, 11422.

(28) (a) Valášek, M.; Pecka, J.; Jindřich, J.; Calleja, G.; Craig, P. R.; Michl, J. *J. Org. Chem.* **2005**, *70*, 405. (b) Berlin, Y. A.; Hutchison, G. R.; Rempala, P.; Ratner, M. A.; Michl, J. *J. Phys. Chem. A* **2003**, *107*, 3970.

(29) Catalan, J.; Garcia de Paz, J. L.; Reichardt, C. *J. Phys. Chem. A* **2010**, *114*, 6226.

(30) (a) Hromadová, M.; Valášek, M.; Fanelli, N.; Randriamahazaka, H. N.; Pospíšil, L. *J. Phys. Chem. C* **2014**, *118*, 9066. (b) Pospíšil, L.;

DOI: 10.1021/jacs.5b05545
J. Am. Chem. Soc. 2015, 137, 11349−11364

Hromadová, M.; Fanelli, N.; Valášek, M.; Kolivoška, V.; Gál, M. *Phys. Chem. Chem. Phys.* **2011**, *13*, 4365.
(31) Frisch, M. J.; et al. *Gaussian 09*, Revision D.01; Gaussian, Inc.: Wallingford, CT, 2009.
(32) Adamo, C.; Barone, V. *J. Chem. Phys.* **1999**, *110*, 6158.
(33) Dunning, T. H., Jr.; Hay, P. J. In *Modern Theoretical Chemistry*; Schaefer, H. F., III, Ed.; Plenum: New York, 1977, Vol. 3, p 1.
(34) Tomasi, J.; Mennucci, B.; Cammi, R. *Chem. Rev.* **2005**, *105*, 2999.
(35) Barone, V. In *Recent Advances in Density Functional Methods*; Chong, D. P., Ed.; World Scientific Publ. Co.: Singapore, 1996; Part 1.
(36) Replacing methyl substituents in *N*-pyridinio Ar^1 moieties by more bulky phenyl groups is aimed at impeding distortion.
(37) Delahay, P. *J. Phys. Chem.* **1966**, *70*, 2373.
(38) de Levie, R.; Pospíšil, L. *J. Electroanal. Chem. Interfacial Electrochem.* **1969**, *22*, 277.
(39) Moreira, H.; de Levie, R. *J. Electroanal. Chem. Interfacial Electrochem.* **1971**, *29*, 353.
(40) Moreira, H.; de Levie, R. *J. Electroanal. Chem. Interfacial Electrochem.* **1972**, *35*, 103.
(41) Sluyters-Rehbach, M.; Sluyters, J. H. *J. Electroanal. Chem.* **1975**, *65*, 831.
(42) Pospíšil, L. *J. Electroanal. Chem. Interfacial Electrochem.* **1976**, *74*, 369.
(43) Marcus, R. A. *J. Chem. Phys.* **1956**, *24*, 966.
(44) Marcus, R. A. *J. Chem. Phys.* **1956**, *24*, 979.
(45) Marcus, R. A. *J. Chem. Phys.* **1965**, *43*, 679.
(46) Hush, N. S. *J. Chem. Phys.* **1958**, *28*, 962.
(47) Levich, V. G. In *Advances in Electrochemistry and Electrochemical Engineering*; Delahay, P., Tobias, C. W., Eds.; Wiley-Interscience: New York, 1966; Vol. 4, p 249.
(48) Dogonadze, R. R. In *Reactions of Molecules at Electrodes*; Hush, N. S., Ed.; Wiley-Interscience: New York, 1971, Chapter 3.
(49) Kuznetsov, A. M. In *Modern Aspects of Electrochemistry*; Bockris, J. O'M.; White, R. E.; Conway, B. E., Eds.; Springer: New York, 1989, Vol. 20, 95.
(50) *Interfacial Electrochemistry*, 2nd ed.; Schmickler, W., Santos, E., Eds.; Springer: New York, 2010.
(51) Pospíšil, L.; Teplý, F.; Gál, M.; Adriaenssens, L.; Horáček, M.; Severa, L. *Phys. Chem. Chem. Phys.* **2010**, *12*, 1550.
(52) Bally, T. *Nat. Chem.* **2010**, *2*, 165.
(53) For simplification and clarity, this main molecular axis (for rodlike forms), running through the $N_{pyridinio}$ and C4 atoms of the pyridinium core, is approximated as being of 2-fold symmetry (e.g. N1−C2 = N1−C6 or C2−C3 = C6−C5, etc.; Figure 3b). For distorted forms, the corresponding mirror replaces the 2-fold axis. The bond-length values used for BL plots are, therefore, mean values taking into account these 2-fold symmetry elements.
(54) Although the great solvation capacity of DMSO is well-recognized, it is also well-established that this solvent behaves more like a Lewis base [donor number (DN) of 29.8, ranking in the top 15 of a scale going from 0.1 to 61] than as a Lewis acid [acceptor number (AN) of 19.3 in a scale going from 0 to 129.1]. In other words, DMSO shows much greater solvation power for cations than for anions. In comparison, while ACN has the same AN as DMSO, its DN is about 2 times smaller (14.1), hence its lower ability to stabilize cations; see the following: Gutmann, V. *Electrochim. Acta* **1976**, *21*, 661.
(55) This flattening/locking process is verified in the following θ values of the saddle-shaped electromer: θ_2 = 5.6°, θ_6 = 5.3°, and θ_1 = 8.0°; see Table S8 in the Supporting Information).
(56) (a) Batsanov, A. S.; Bryce, M. R.; Coffin, M. A.; Green, A.; Hester, R. E.; Howard, J. A. K.; Lednev, I. K.; Martín, N.; Moore, A. J.; Moore, J. N.; Ortí, E.; Sánchez, L.; Savirón, M.; Viruela, P. M.; Viruela, R.; Ye, T.-Q. *Chem. - Eur. J.* **1998**, *4*, 2580. (b) Bryce, M. R.; Moore, A. J.; Hasan, M.; Ashwell, G. J.; Fraser, A. T.; Clegg, W.; Hursthouse, M. B.; Karaulov, A. I. *Angew. Chem., Int. Ed. Engl.* **1990**, *29*, 1450. (c) Bryce, M. R.; Coffin, M. A.; Hursthouse, M. B.; Karaulov, A. I.; Müllen, K.; Scheich, H. *Tetrahedron Lett.* **1991**, *32*, 6029.
(57) Bendikov, M.; Wudl, F.; Perepichka, D. F. *Chem. Rev.* **2004**, *104*, 4891 and references therein.
(58) (a) Schubert, U.; Hünig, S.; Aumüller, A. *Liebigs Ann. Chem.* **1985**, *1985*, 1216. (b) Kabuto, C.; Fukazawa, Y.; Suzuki, T.; Yamashita, Y.; Miyashi, T.; Mukai, T. *Tetrahedron Lett.* **1986**, *27*, 925. (c) Heimer, N. E.; Mattern, D. L. *J. Am. Chem. Soc.* **1993**, *115*, 2217.
(59) Gomez, R.; Seoane, C.; Segura, J. L. *Chem. Soc. Rev.* **2007**, *36*, 1305 and references therein.
(60) Kurata, H.; Tanaka, T.; Oda, M. *Chem. Lett.* **1999**, 749.
(61) There exist also examples of rodlike systems at the ground state that, conversely, adopt saddle-shaped distortion in their photoexcited state; see the following: Ciofini, I.; Adamo, C.; Teki, Y.; Tuyèras, F.; Lainé, P. P. *Chem. - Eur. J.* **2008**, *14*, 11385.
(62) It should be noted that, in the case of **4**, there is room for further potential separation (i.e., "expansion") if the steric hindrance of Ar^1 is further increased so as to strictly keep the axial geometry in the $[Z - 2]$ state.
(63) We have shown that, for tuning the standard potentials, playing on steric parameters is at least as efficient as playing, more conventionally, on electronic factors via electron-donating/withdrawing substituents. Thus, choosing the steric hindrance pattern allows one to decide (1) if electrophores will transfer (uptake/release) electrons sequentially or "at once" (via the tuning of the level of local congestion around the Ar^1 *N*-pyridinio group of the pyridinium core) and (2), in the latter case, the degree of reversibility of the two-electron transfer (via the tuning of the level of overall congestion around the pyridinium core).
(64) (a) Kang, H.; Facchetti, A.; Zhu, P.; Jiang, H.; Yang, Y.; Cariati, E.; Righetto, S.; Ugo, R.; Zuccaccia, C.; Macchioni, A.; Stern, C. L.; Liu, Z.; Ho, S.-T.; Marks, T. J. *Angew. Chem., Int. Ed.* **2005**, *44*, 7922. (b) Albert, I. D. L.; Marks, T. J.; Ratner, M. A. *J. Am. Chem. Soc.* **1998**, *120*, 11174.

DOI: 10.1021/jacs.5b05545
J. Am. Chem. Soc. 2015, 137, 11349−11364